Nano Research

ISSN 1998-0124 CN 11-5974/O4
https://doi.org/10.26599/NR.2026.94908741

Review Article

Self-powered sensors driven by osmotic energy: From fundamentals to applications

Wenhao Shi[1], Jincheng Wu[2], Zijun Li[2], Xiaoguang Hu[2](✉), Longlu Wang[1,2](✉)

[1] School of Communications and Information Engineering, Nanjing University of Posts and Telecommunications (NJUPT), Nanjing 210023, China

[2] College of Electronic and Optical Engineering and College of Flexible Electronics (Future Technology), Nanjing University of Posts and Telecommunications (NJUPT), Nanjing 210023, China

Nano Res., **Just Accepted Manuscript** • https://doi.org/10.26599/NR.2026.94908741

https://www.sciopen.com/journal/1998-0124 on Apr. 16, 2026

Just Accepted

Nano Research

TABLE OF CONTENTS (TOC)

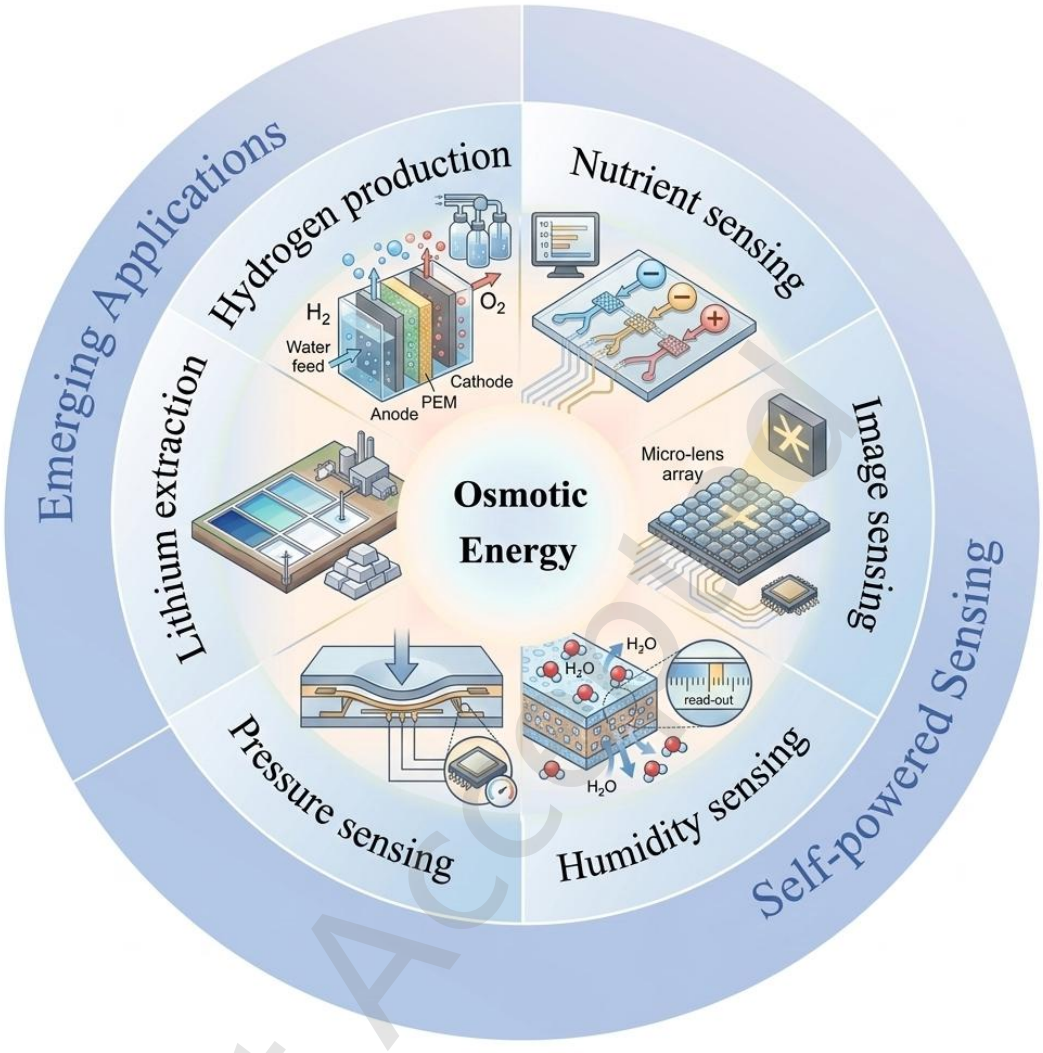

This review systematically summarizes osmotic energy-driven integrated self-powered sensors, covering their fundamentals, design strategies, and analyzes sensing mechanisms in nutrient/pressure/humidity/image sensing, and emerging applications driven by osmotic energy (lithium extraction, hydrogen production). The future development directions and challenges are also discussed.

Nano Research

Open Access

Review Article

Self-powered sensors driven by osmotic energy: From fundamentals to applications

Wenhao Shi[1], Jincheng Wu[2], Zijun Li[2], Xiaoguang Hu[2] ✉, and Longlu Wang[1,2] ✉

[1]*School of Communications and Information Engineering, Nanjing University of Posts and Telecommunications (NJUPT), Nanjing 210023, China*

[2]*College of Electronic and Optical Engineering and College of Flexible Electronics (Future Technology), Nanjing University of Posts and Telecommunications (NJUPT), Nanjing 210023, China*

Received: 10 March 2026; **Revised:** 3 April 2026; **Accepted:** 16 April 2026

✉ Address correspondence to Longlu Wang, wanglonglu@hnu.edu.cn; Xiaoguang Hu, xghu@njupt.edu.cn

Cite this article: *Nano Research*, 2026, 19, 94908741 https://doi.org/10.26599/NR.2026.94908741

ABSTRACT: With the rapid development of nanofluidic materials and the urgent demand for low-power self-sustaining sensing systems, developing osmotic energy-driven self-powered sensors has become a research focus. Osmotic energy, a promising blue energy with enormous reserves, has long been underutilized due to the limitations of traditional harvesting technologies. In contrast, integrated self-powered sensing driven by osmotic energy achieves seamless integration of energy conversion and sensing via advanced nanofluidic membranes and selective ion transport, exhibiting superior miniaturization and efficient signal transduction. However, previous research focuses on separated design of such systems, a systematic review focusing on the integrated design of osmotic energy-driven self-powered sensing remains lacking. Herein, we first summarize its fundamentals, including the osmotic energy conversion mechanism, advanced nanomaterials for ion-selective membranes as well as their selection criteria. Next, typical sensing applications in nutrient, pressure, humidity and image sensing are discussed, with emphasis on the specific sensing mechanisms underlying each category, such as light-regulated surface charge density for image sensing. Additionally, other emerging applications like self-powered lithium extraction and hydrogen production are presented. Finally, critical challenges and future research directions are proposed, aiming to guide the practical development and large-scale integration of such sensing systems.

KEYWORDS: osmotic energy, self-powered, flexible sensing, lithium extraction, hydrogen production

1. Introduction

Osmotic energy, harnessed from the salinity gradient between seawater and freshwater, stands out as a highly promising renewable energy source for the global carbon neutrality transition [1-8]. Boasting a theoretical global reserve of over 30 terawatts [9], it features unique advantages of stable output independent of weather conditions, complementing intermittent energy sources such as wind and solar power [10-13]. Despite its enormous energy potential, however, osmotic energy has long remained drastically underutilized in practical applications [14-18]. This predicament stems from the inherent limitations of traditional osmotic energy harvesting technologies including pressure-retarded osmosis (PRO) and reverse electrodialysis (RED) [19-24], such as low power density [25, 26], exorbitant membrane material costs [27-29], and an inescapable trade-off between membrane permeability and selectivity [30-32]. These drawbacks have prevented this abundant energy source from being integrated into the renewable energy application system. Fortunately, the development of biomimetic nanofluidic channels has brought a pivotal breakthrough for the efficient utilization of osmotic energy: these channels mimic the selective ion transport behavior of biological ion channels to achieve efficient osmotic energy conversion [33-41]. Recent advances in 1D nanotubes, 2D layered materials, and 3D porous frameworks have further greatly improved ion selectivity and permeability, pushing the power density of osmotic energy devices to unprecedented heights [24, 41-48]. These technological breakthroughs have not only unlocked the practical application potential of osmotic energy but also laid a solid foundation for its integration with sensing technology. The rise and development of osmotic energy-driven self-powered sensing technology is an excellent proof of the practical application value of osmotic energy, and has become an important research achievement in this field.

As a typical “blue energy” source, osmotic energy conversion relies on the selective transport of ions across functional membranes to convert chemical potential energy from salinity gradients into electrical energy [49-52]. The core component of this process is the ion-selective membrane [53-55], whose performance is dominated by the electric double layer (EDL) effect within nanoscale channels [56-61]. When the channel size is comparable to the Debye length, the EDL formed on the membrane surface overlaps significantly, leading to the preferential adsorption of counterions and effective repelling of co-ions. This selective ion transport mechanism, derived from electrostatic interactions and steric hindrance, is the fundamental basis for osmotic energy conversion and subsequent self-powered

sensing. Early ion-selective membranes, such as cation-exchange membranes (CEMs) and anion-exchange membranes (AEMs) used in RED systems [62-65], suffer from low ion selectivity and high transport resistance. The development of nanomaterial-based membranes, including graphene oxide (GO) membranes [66], metal-organic framework (MOF) membranes [67], and layered double hydroxide (LDH) composite membranes [68], has revolutionized this field. These advanced membranes feature well-defined nanochannels, high surface charge density, and tunable pore structures, which significantly enhance ion selectivity and permeability. For example, NiAl-LDH coated anodic aluminum oxide (NiAl-LDH@AAO) composite membranes exhibit intrinsic anion selectivity due to positively charged LDH layers, enabling efficient osmotic energy conversion under salinity gradients [69]. The precise regulation of membrane properties provides a flexible platform for the design of high-performance osmotic energy devices and their integration with sensing functions.

The rapid development of Internet of Things (IoT) and wearable electronics has spurred an urgent demand for low-power [70, 71], cost-effective and portable sensing systems [72-77]. Among various self-powered platforms [78, 79], osmotic energy-driven self-powered sensors, which convert chemical potential energy from salinity gradients into electrical signals for sensing, have emerged as a promising solution to this challenge [80]. These sensing systems can be categorized into two types: separated self-powered sensors and integrated self-powered sensors. Separated systems employ independent osmotic energy generators to supply power to external sensors, which suffer from complex structures, energy loss during transmission, and poor miniaturization potential. In contrast, integrated self-powered sensors are those devices in which the sensing element itself simultaneously acts as the energy converter. The concentration gradient employed by such sensors can originate from either the external environment or a built-in source, and the choice between them is typically determined by practical application scenarios. The use of an external or built-in gradient does not affect the classification of integration, as long as the single element serves as both the sensing and energy-converting unit. This integration eliminates the need for additional power modules and transmission components, enabling miniaturization, reduced energy loss, and enhanced structural stability. Moreover, the intrinsic coupling between ion transport and sensing responses in integrated systems allows for direct signal transduction, improving sensing sensitivity and response speed.

The superior performance of integrated self-powered sensors stems from their structural and functional synergy. Firstly, the shared material platform ensures that the energy conversion and sensing processes are regulated by the same ion transport mechanism, enabling efficient signal transduction. For example, in pressure sensing systems based on 2D nanofluidic membranes, external pressure modulates interlayer spacing to simultaneously alter ion transport efficiency and generate distinguishable electrical signals [81]. Secondly, the integrated design minimizes interfacial resistance and energy dissipation associated with external circuits, significantly improving the overall energy utilization efficiency [82]. Additionally, the compact structure of integrated sensors facilitates their application in confined spaces, such as wearable devices and in-situ environmental monitoring [83]. Their inherent self-powered merit also extends the service life of sensing systems, making them suitable for long-term unattended monitoring in remote areas.

Despite these advances, the research on osmotic energy-driven integrated self-powered sensors remains in its fancy, with several critical challenges to be addressed. Current studies in this field mostly focus on separated self-powered sensors, lacking systematic analysis of integrated devices and in-depth discussion on their core design concepts, material optimization strategies or sensing mechanisms. This review aims to provide a comprehensive overview of osmotic energy-driven integrated self-powered sensing systems. First, the fundamentals of osmotic energy conversion, including energy conversion mechanisms, advanced membrane materials and selection criteria for them, are elaborated. Then, through Table 1, the design strategies, sensing mechanisms and performance of integrated sensors in major application fields (nutrient, pressure, humidity, image sensing), as shown in Figure 1, are systematically discussed. Subsequently, other emerging applications of osmotic energy-driven self-powered technology, such as self-powered lithium extraction and hydrogen production, are also presented. Finally, current challenges and future research directions, including material innovation, structural optimization, and large-scale integration, are analyzed. This review offers valuable insights for researchers in materials science, energy engineering, and sensor technology, promoting the development of high-performance integrated self-powered systems.

Nano Research

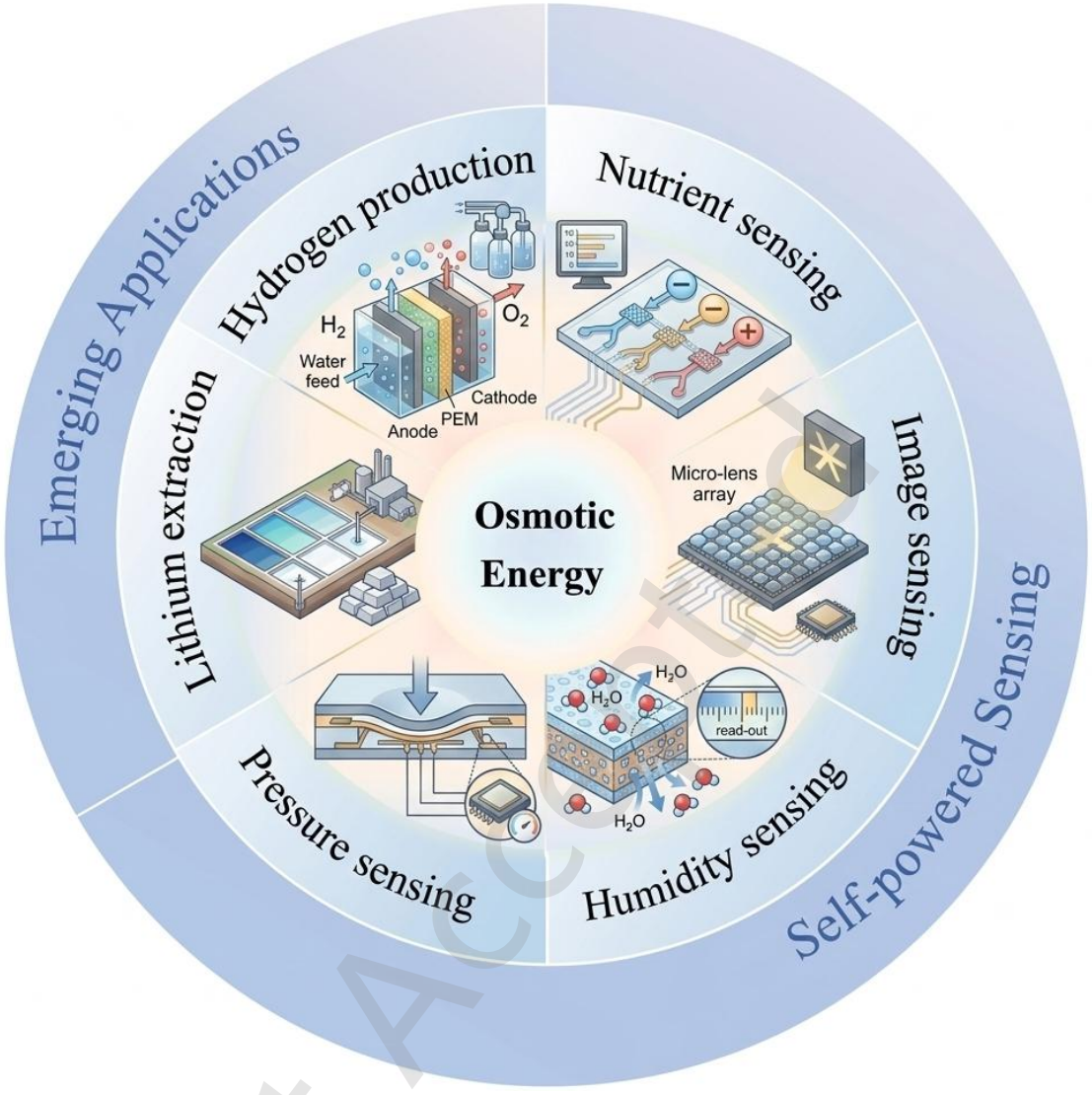

Figure 1. Schematic illustration of the application driven by osmotic energy, including self-powered sensing.

2. Fundamental of osmotic energy-driven self-powered systems

2.1 Energy conversion mechanisms

The energy conversion of osmotic energy-driven self-powered sensing is fundamentally governed by the EDL effect and ion-selective transport dynamics, forming a seamless link between salinity gradient potential and usable electrical energy for sensing. When high-concentration solutions and low-concentration solutions are separated by ion-selective nanofluidic membranes, the membrane's surface charges derived from functional groups or material intrinsic properties, interact with electrolyte ions to form EDLs at the membrane-solution interface. As illustrated in Figure 2, each EDL consists of a Stern layer and a diffusion layer. The characteristic thickness of the EDL, known as the Debye length (λ_D), is determined by the electrolyte concentration and temperature, typically ranging from a few nanometers to tens of nanometers. It is mathematically defined by the Equation 1:

$$\lambda_D = \sqrt{\frac{k_B T}{e^2 \sum_i z_i^2 n_i}} \#(1)$$

In this expression, k_B denotes the Boltzmann constant, T is the absolute temperature, e represents the elementary charge, z_i is the valence of the i-th ionic species, and n_i is the number density of the i-th ionic species in the electrolyte solution.

Figure 2 vividly demonstrates the relationship between nanochannel radius and EDL overlap behavior across three distinct scenarios. For wide-radius channels, the channel width far exceeds the λ_D, so the EDLs on opposite channel walls remain not overlap. In this case, co-ions can freely diffuse into the channel center, resulting in weak ion selectivity. For intermediate-radius channels, the channel size matches the λ_D, making EDLs from both channel walls begin to overlap. This overlap creates a continuous electrostatic field that fills the entire channel, where counterions are highly concentrated in the channel interior while co-ions are effectively excluded, maximizing ion selectivity. For narrow-radius channels, the channel width is smaller than the λ_D, resulting in fully overlapped EDLs that completely dominate the channel space. In this scenario, co-ions are almost entirely repelled from the channel, and counterions become the exclusive charge carriers, achieving the highest level of ion perm-selectivity. This size-dependent EDL overlap behavior directly modulates the ion transport environment, laying the physical foundation for converting the chemical potential energy of the salinity gradient into electrical energy.

Beyond the classical EDL effect, ion transport in confined nanofluidic systems is governed by multi-scale mechanisms at the structural, interfacial, atomic and electronic levels, which provide critical guidance for the design of osmotic energy-driven self-powered sensing systems. For 2D layered nanofluidic membranes most widely used for osmotic energy conversion, ions are transported via three typical pathways: vertical transport through nanopores of single

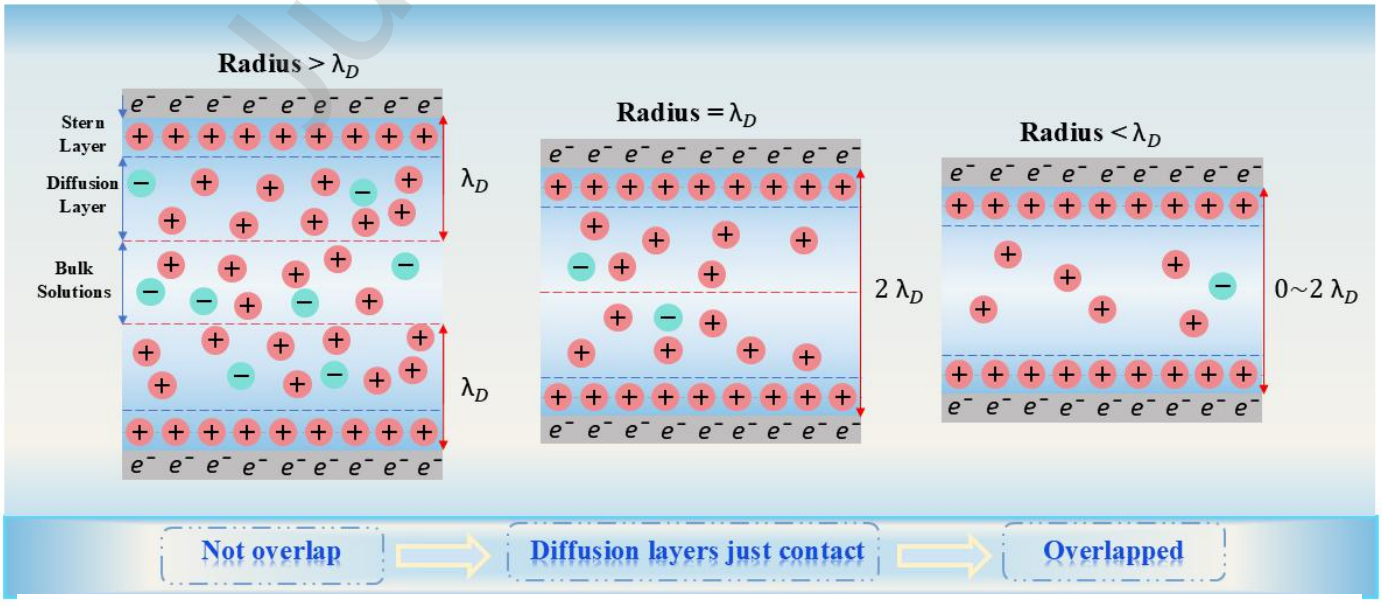

Figure 2. Schematic illustration of EDL overlap behavior in nanofluidic channels with different radii.

nanosheets, horizontal transport along interlayer gaps of stacked nanosheets, and composite transport through the interpenetrating network of the two channels [2]. These channels are generally sub-nanometer scaled, and the traditional EDL theory requires substantial supplementation and extension to describe ion transport at this scale. The classical EDL model has two inherent limitations. First, it simplifies ions in the Stern layer as point charges and neglects the critical role of ionic size. Moreover, its core assumption that surface charge determines ion selectivity fails to explain the selective transport dominated by ion-membrane binding energy in electrically neutral 2D materials. However, the electrostatic interaction between interfacial surface charges and ions revealed by the classical EDL theory remains the fundamental physical basis for confined ion transport. At the solid-liquid interface, ion transport exhibits significant valence-dependent behavior [84]. The transport capacity of divalent cations is remarkably inferior to that of monovalent cations, which can be fully explained by the interfacial binding rope theory. The stronger electrostatic attraction between divalent cations and negatively charged pore walls, combined with the rearranged hydration shell structure and interfacial hydrogen bond interactions, collectively enhances the interfacial binding effect and hinders ion migration. At the atomic scale, existing studies have also identified distinct transport mechanisms for different ions. Hydrated Cl^- migrate via the vehicular mechanism, moving as a whole with constant identity, while OH^- follow the mixed vehicular-Grotthuss mechanism, where frequent proton transfer between adjacent water molecules enables ion hopping with a significantly reduced migration energy barrier [85]. In addition, the intrinsic electronic properties of channel materials play a non-negligible role in regulating ion transport: at the same surface charge density, semiconducting channel materials exhibit lower liquid-solid friction and higher ion mobility than metallic materials, originating from the quantum electrokinetic coupling between the electronic degrees of freedom of solids and the fluctuation of interfacial water molecules [86]. The above multi-scale regulatory mechanisms collectively determine the ion transport efficiency and the subsequent osmotic energy conversion process.

The specific energy conversion process relies on the directional migration of counterions driven by the chemical potential difference between high and low concentrations, with the EDL overlap effect ensuring the formation of a net ion flux and transmembrane potential. The theoretical maximum osmotic energy (dG) available for powering sensing processes is quantified by the thermodynamic Equation 2:

$$\mathrm{d}G = -\frac{RT}{F} ln \frac{\tau_H}{\tau_\mathrm{L}} (|I_+| + |I_-|) dt \#(2)$$

where R is the universal gas constant, T is the absolute temperature (in Kelvin), F is the Faraday constant, τ_H and τ_L are the activities of high- and low-concentration electrolytes, respectively, and I_+、I_- represent the diffusion currents of cations and anions. This equation indicates that the available energy is positively correlated with the concentration difference and the net ion flux, where counterions (the primary charge carriers due to EDL-induced selectivity) dominate the energy output. For practical sensing applications, the actual usable power is determined by the maximum power density (P_{max}) of the conversion system, which is derived from the osmotic potential (E_{osm}) and membrane internal resistance (R_M), as shown in Equation 3:

$$P_{max} = \frac{E_{\mathrm{osm}}^2}{4R_\mathrm{M}} \#(3)$$

Here, E_{osm} is equivalent to the Nernst potential across the membrane, which depends on the salinity gradient and ion selectivity enhanced by EDL overlap. R_M is influenced by the channel length, pore density, and ion mobility within the membrane, with the EDL overlap effect reducing ion transport resistance by concentrating counterions in the channel. Electrodes placed in the high and low concentration electrolytes play a critical role in this process. They mediate redox reactions to maintain system electroneutrality, enabling continuous ion migration and converting the net ion flux into a stable electrical current in the external circuit that directly powers the sensing element. This integration of EDL-induced ion selectivity and thermodynamic energy conversion ensures efficient and sustained self-power supply for sensing systems.

Notably, as the core driving force for osmotic energy conversion, the ion concentration gradient critically governs

ion transport behavior and output power performance, which are jointly regulated by the surface charge density within nanochannels and the bulk electrolyte concentration. In the low-concentration gradient, the λ_D is comparable to or larger than the characteristic dimension of nanochannels, enabling fully overlapped EDLs inside the channels. Ion transport is thus dominated by surface charge effects with exceptional ion selectivity. The output power remains relatively low due to the limited driving force. With an increasing concentration gradient, the thermodynamic driving force is substantially enhanced, giving rise to remarkable improvements in ion flux and output power, yet the λ_D on the high-concentration side decreases, compressing the EDL thickness, weakening ion selectivity, and creating a bulk-like central region unaffected by surface charge, so that ion transport becomes governed by the chemical potential difference derived from the concentration gradient. Notably, a higher concentration gradient provides stronger driving force but simultaneously aggravates interfacial ion concentration polarization (ICP) [87], which compromises energy conversion efficiency and causes output power to rise first and then decline, and introducing charge-gradient structures can generate a built-in electric field to accelerate ion transport and mitigate polarization-induced resistance for maintaining high efficiency under large concentration gradients [88]. Nevertheless, when the system enters an ultrahigh-concentration gradient regime, the high-salinity electrolyte enters the water-in-salt (WIS) state or even transforms into a neat ionic liquid system, where classical dilute-solution EDL theories are no longer valid because strong ion correlation effects and hierarchical concentration distributions emerge in highly concentrated aqueous electrolytes, leading to deviations of ion transport from the classical Nernst-Einstein relation [89], and ionic liquids exhibit unique oscillatory layered aggregation and anisotropic interfacial dynamics [90]. these complex interfacial structures and transport behaviors cannot be accurately described by conventional theoretical frameworks, indicating that further systematic investigations focusing on ultrahigh-concentration systems and ionic liquid-based interfaces are urgently required to establish more accurate predictive models for ion transport and energy conversion efficiency.

2.2 Advanced materials for membranes

Ion-selective nanofluidic membranes are the core component of osmotic energy-driven self-powered systems. Their ion transport selectivity, permeability, and environmental adaptability directly determine the energy conversion efficiency and long-term stability of the devices [91]. These membrane materials achieve selective ion transport under salinity gradients by virtue of well-defined nanoscale channels and tailored surface charge properties [92, 93]. They lay the foundation for energy harvesting and sensing functions. Based on structural characteristics and material compositions, the advanced nanofluidic membranes widely studied currently mainly include 2D layered membranes and 3D porous framework membranes as shown in Figure 3. Each category of materials possesses distinct advantages and inherent limitations.

2D layered membranes have become the most widely applied type of nanofluidic membrane in sensing systems due to their balanced performance in ion selectivity, processability, and compatibility with flexible device integration. These membranes form interlayer nanofluidic channels through the stacking of nanosheets. They cover representative materials such as GO membranes [94], MXene membranes [95], and layered LDH nanosheet membranes [68]. MXene membranes exhibit outstanding performance in interlayer spacing tunability and high surface charge density. Interlayer spacing can be precisely regulated through physical compression or chemical modification. This regulation makes it comparable to the λ_D in solutions, thereby realizing ion-selective transport based on charge repulsion. Abundant surface functional groups such as $-O^-$, -OH, and -F endow MXene membranes with high negative charge density and strong cation selectivity [96, 97]. The surface of GO membranes is also rich in oxygen-containing functional groups [98, 99]. Hydroxyl and epoxy groups are

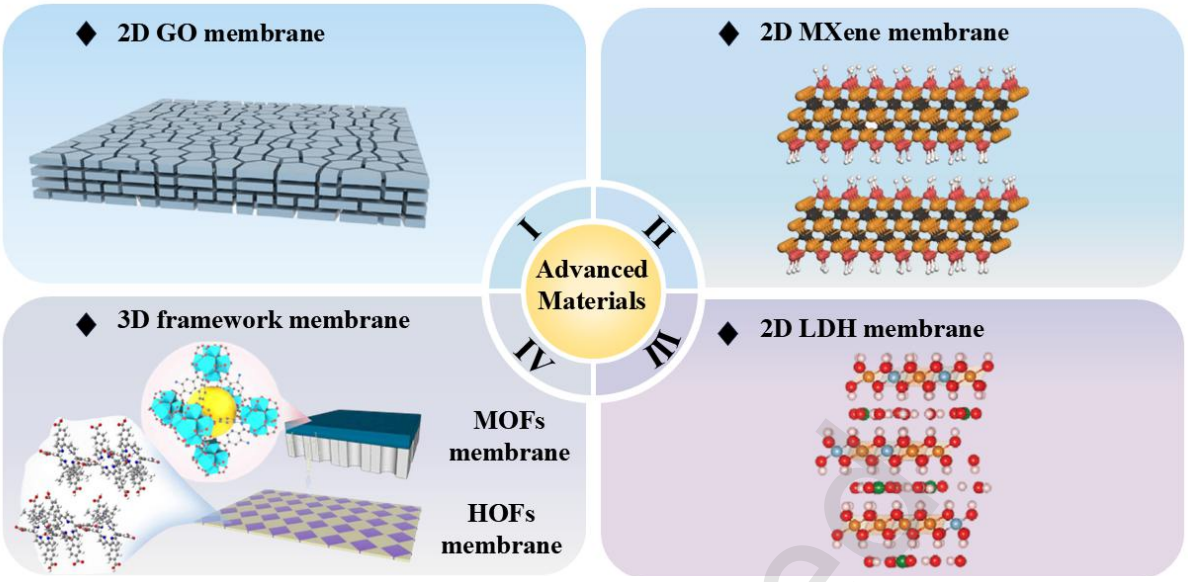

Figure 3. Advanced membrane materials for self-powered systems driven by osmotic energy. (Reproduced with permission from Ref [94], Copyright 2023, Wiley-VCH Verlag. Reproduced with permission from Ref. [95], Copyright 2024, Wiley-VCH Verlag. Reproduced with permission from Ref. [68], Copyright 2023, Wiley-VCH Verlag. Reproduced with permission from Ref. [109], Copyright 2021 American Association for the Advancement of Science. Reproduced with permission from Ref. [110], Copyright 2022, American Chemical Society.)

distributed on the basal plane, while carboxyl groups are abundant at the edges. These groups dissociate in aqueous environments. This dissociation makes the surface of GO membranes negatively charged and endows them with a certain degree of cation selectivity. However, their charge density is usually lower than that of MXene. The charge density and ion selectivity of GO membranes can be further improved through chemical modifications such as carboxylation and sulfonation [100, 101]. But these modifications increase the complexity of preparation. LDH membranes are a unique type of anion-selective 2D layered material. Their laminates carry positive charges, and exchangeable anions can be accommodated between the layers [102, 103]. Thus, they can efficiently transport anions while repelling cations. This fills the gap in the development of anion-selective membranes. LDH membranes are usually prepared on porous substrates such as AAO by in-situ growth. This composite structure integrates the mechanical stability of the substrate and the ion selectivity of LDH. It ensures the structural integrity of the device under repeated stimuli. In addition, 2D layered membranes can be prepared by methods such as vacuum filtration [104], spin coating [105], or in-situ growth [106]. These methods provide convenience for practical applications. However, 2D layered membranes also have inherent drawbacks. For MXene and GO membranes, the combination between nanosheets relies on weak van der Waals forces [107, 108]. This leads to poor mechanical stability. They are prone to swelling in high-humidity environments, which reduces ion selectivity. For LDH composite membranes, the growth of LDH nanosheets may excessively narrow the substrate channels. This increases ion transport resistance. Moreover, their ion selectivity is highly sensitive to pH. Performance is prone to degradation in alkaline environments. In addition, the large-scale synthesis of uniform LDH layers still faces technical challenges. This limits their commercial promotion. The tortuous transport paths between the layers of 2D layered membranes also increase ion transport resistance. This restricts the further improvement of energy conversion efficiency.

3D porous framework membranes such as HOF membranes and MOF membranes have interconnected nanochannel networks and ultrahigh specific surface areas [109, 110]. They exhibit unique advantages in osmotic energy conversion by virtue of customizable pore structures [111, 112]. HOF membranes are formed by the self-assembly of organic monomers through reversible hydrogen bonds [113]. As a representative of metal-free crystalline porous

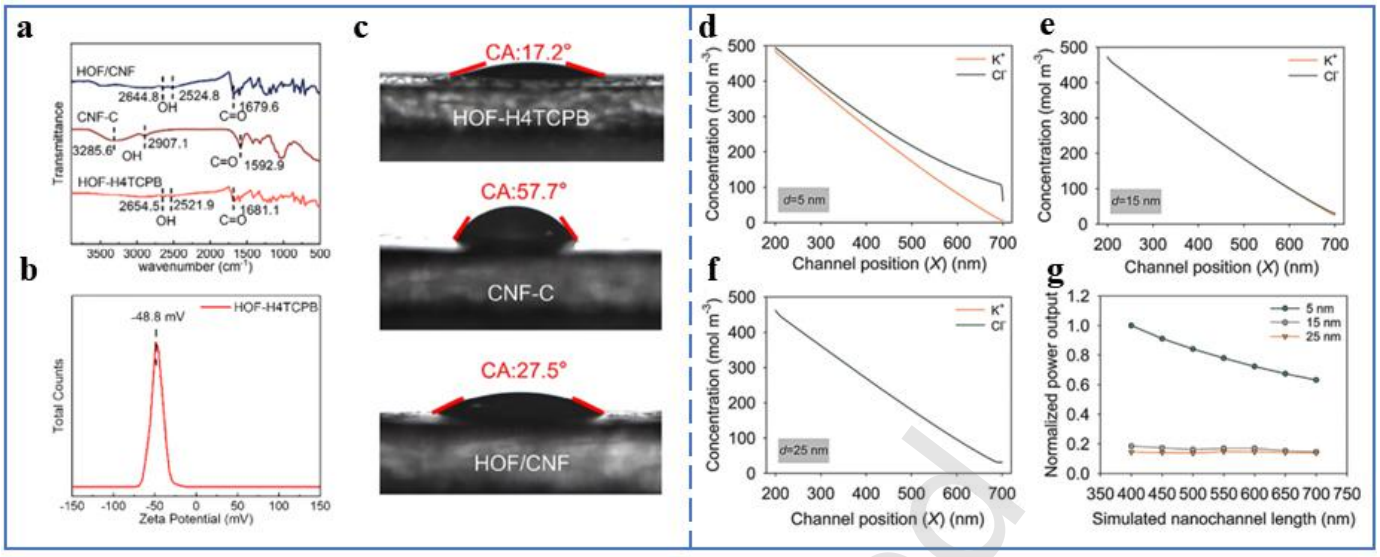

Figure 4. (a) FTIR spectra of HOF-H4TCPB, CNF-C, and H4TCPB membranes. (b) Zeta potential measurement of HOF-H4TCPB suspension. (c) Contact angle images of HOF-H4TCPB, CNF-C, and HOF/CNF membranes. (Reproduced with permission from Ref. [102] Copyright 2022, Wiley-VCH Verlag.) (d) Average cation and anion concentration profiles along the nanofluidic channel with a radius of 5 nm (simulation results). (e) Average cation and anion concentration profiles along the nanofluidic channel with a radius of 15 nm (simulation results). (f) Average cation and anion concentration profiles along the nanofluidic channel with a radius of 25 nm (simulation results). (g) Calculated normalized power output of nanofluidic channels with various channel sizes and lengths (simulation results). (Reproduced with permission from Ref. [69], Copyright 2022, Wiley-VCH Verlag.).

materials, they possess uniform pore structures [113], large specific surface areas [114], and tunable pore morphologies and sizes [115]. The potential for surface modification further enhances their performance in ion-selective transport and osmotic energy conversion. Uniformly distributed hydrogen bonding sites endow HOF membranes with unique environmental response characteristics. The presence of a large number of reversible hydrogen bonds results in significant differences in their ion transport performance under high-humidity and low-humidity environments. They exhibit rapid humidity response and stable ion selectivity. However, 3D porous framework membranes face challenges in practical applications. MOF materials are prone to structural hydrolysis in aqueous environments, leading to insufficient long-term durability [116]. HOF membranes have weak mechanical strength. They are often compounded with reinforcing materials such as cellulose nanofibers (CNF) to improve toughness. In addition, the synthesis of framework materials often involves complex processes and toxic solvents. This increases preparation costs and environmental burdens.

2.3 Selection criteria for membranes

The rational selection of ion-selective nanofluidic membranes is critical to the performance optimization of osmotic energy-driven self-powered sensing systems. The selection process should comprehensively consider key material properties that directly govern ion transport efficiency, energy conversion stability, and sensing responsiveness, including surface charge characteristics (surface charge density, zeta potential), nanochannel structural parameters (radius and length), and hydrophilicity. Surface charge acts as the primary determinant of ion selectivity, while other criteria synergistically regulate ion transport kinetics and practical applicability.

Surface charge provides the essential basis for selective ion transport and mainly depends on functional modification to introduce charged groups. A central selection principle is to match the membrane charge polarity with the target ion type: negatively charged membranes favor cation transport, whereas positively charged membranes enable anion selectivity. For example, the HOF-H4TCPB membrane used in self-powered humidity sensor carries abundant carboxyl groups (Figure 4a), and shows a zeta potential of approximately -48.8 mV (Figure 4b), providing strong negative charge for efficient cation migration. Currently,

anion-selective membranes with stable positive charge are still insufficient, limiting the expansion of sensing applications. Sustaining charge stability under working conditions is also essential to maintain consistent ion selectivity.

Hydrophilicity acts as a key complementary factor that ensures unobstructed ion transport pathways. While surface charge offers the driving force for ion selectivity, hydrophilicity promotes water adsorption and hydrated ion migration, especially in aqueous or humid environments. The HOF-H4TCPB membrane exhibits excellent hydrophilicity with a contact angle of 17.2° (Figure 4c), which accelerates ion flux and response speed. After compounding with HOF-H4TCPB, the hydrophilicity of CNF-C is significantly improved, which helps homogenize charge distribution and reduce interfacial ion aggregation.

Nanochannel radius serves as a crucial structural parameter that amplifies ion selectivity through the EDL overlap effect. For effective selection, the channel radius should be tuned to match the λ_D under target operating conditions. Studies on LDH@AAO anion-selective membranes ultilized for nutrient sensing demonstrate that a channel radius of 5 nm supports full EDL overlap and outstanding ion selectivity (Figure 4d), whereas selectivity gradually diminishes as the radius increases to 15 nm and 25 nm (Figure 4e, f). Therefore, adjusting the channel radius to enter the EDL overlap region is a critical criterion for achieving high-performance ion-selective membranes.

Nanochannel length further balances ion flux and energy conversion efficiency, which cannot be resolved by charge and hydrophilicity alone. A shorter channel reduces migration resistance but may impair selectivity; a longer channel enhances electrostatic interactions but increases energy loss. Simulations based on LDH@AAO membranes reveal that the normalized power output decreases notably with increasing channel length at a radius of 5 nm (Figure 4g), while larger radii show a trade-off between selectivity and conductance. Thus, channel length should be optimized according to the required flux and sensitivity for specific sensing scenarios.

In summary, the core selection criteria for ion-selective nanofluidic membranes exhibit distinct characteristics and synergistic relationships in regulating ion transport and sensing performance. Surface charge, achieved through functional modification and matched to target ion polarity, lays the foundation for ion selectivity, with anion-selective membranes requiring further development. Hydrophilicity optimizes transport kinetics, while nanochannel radius and length, as structural parameters, further tailor selectivity and flux to match practical application demands. A comparative analysis of these criteria, considering factors such as modification feasibility, environmental adaptability, and structural tunability, provides valuable guidance for the rational design of high-performance membranes for self-powered sensing systems.

3. Osmotic energy-driven self-powered sensing

3.1 Nutrient sensing enabled by 2D NiAl-LDH

Ion concentration detection represents a direct application of osmotic energy conversion in nanofluidic systems. Since osmotic power generation arises from salinity gradients, the electrical output of ion-selective nanochannels inherently depends on ionic concentration. This coupling enables concentration sensing without external power input. Thus, the sensing of nutrients in hydroponic agriculture can be achieved by detecting specific ions in the nutrient solution. However, stable and quantitative detection requires controlled nanochannel structure and defined surface charge characteristics to ensure selective ion transport.

In this context, Liu et al. [69] reported a NiAl-LDH@AAO composite membrane prepared by a precipitant-free in situ growth strategy. Figure 5a schematically illustrates the osmotic power generation and anion-selective transport mechanism of the NiAl-LDH@AAO composite membrane, where positively charged LDH layers repel cations, while anions pass through the nanochannels driven by the salinity gradient. EDX elemental mapping results for Na^+ and Cl^- further confirm the composite membrane's anion selectivity, with Cl^- highly enriched in the nanochannels, while Na^+ show almost negligible signals due to electrostatic repulsion. The cross-sectional SEM image in Figure 5b clearly reveals the dense, parallel growth of LDH sheets along the inner surfaces of the AAO nanochannels. This growth process not only narrows the original pore size of the

Table 1 Key characteristics of self-powered sensors driven by osmotic energy.

Sensing type	Working mechanism	Nanofluidic membrane materials	Concentration gradient construction	Signal response manner
Nutrient sensing [69, 87]	Nutrient anion concentration-governed selective transport	(1) NiAl-LDH@AAO (2) polypyrrole-GO	External environmental salinity gradient	Nutrient ion concentration → anion/ cation flux → short-circuit current
Pressure sensing [81]	Pressure-modulated interlayer spacing and EDL overlap	KOH-modified GO / GO	Built-in gradient inside the membrane	Pressure → cation flux → open-circuit voltage
Humidity sensing [117]	Humidity-regulated water adsorption and ion migration barrier	HOF/ CNF	Built-in gradient inside the membrane	Humidity → Na^+ flux → current density
Image sensing [125]	Light-modulated surface charge density and ion entrance barrier	Photoacid-grafted GO	Built-in gradient inside the sensor (outside the membrane)	Light illumination → cation flux → ionic current

AAO template and increases the effective length of the nanochannels but also modulates the membrane's ion conductivity by establishing a positively charged interface. The practical performance of the composite membrane is also influenced by external environmental factors. In practical tests, the power density of the composite membrane in sodium chloride solution decreases steadily as pH rises from 3 to 11, indicating that acidic conditions favor the retention of higher positive surface charge density. This is attributed to the decrease in Zeta potential of NiAl-LDH with increasing pH, leading to a reduction in the membrane's positive surface charge density. This finding further demonstrates that the membrane is pH-responsive, suggesting potential for future pH sensing applications. In terms of overall performance, Figure 5c categorizes existing nanofluidic membranes into negatively charged, positively charged, and bipolar types. The NiAl-LDH@AAO composite membrane shows excellent output power density and energy conversion efficiency among positively charged anion-selective membranes. Its straightforward fabrication method, which requires no chemical modifications, further underscores its application advantages. For practical hydroponic ion concentration sensing, a real-time self-powered detection system based on this composite membrane was developed, as shown in Figure 5d. This device presents a fully integrated structure and belongs to a typical integrated self-powered sensor. For hydroponic agricultural monitoring, the external nutrient concentration gradient is an inherent environmental condition rather than an independent energy harvester, and whether a built-in or external gradient is used depends on the actual application scenario instead of determining the integration property. The ion-selective nanofluidic membrane itself undertakes both osmotic energy conversion and nutrient concentration sensing simultaneously, fully complying with the definition of integrated design. This system, consisting of the NiAl-LDH@AAO composite membrane and an electrometer data acquisition board, successfully collects and transmits the electrical signal generated by osmotic energy conversion. Figure 5e shows the measured short-circuit current and conductivity values for various nutrient solution concentrations, confirming that the short-circuit current generated by the system is significantly positively correlated with nutrient concentration and can serve as a direct indicator of ion concentration. Long-term monitoring of romaine lettuce cultivation (Figure 5f) further validates the practical sensing capability of the system. During the 7-day monitoring period, the trend of the measured short-circuit

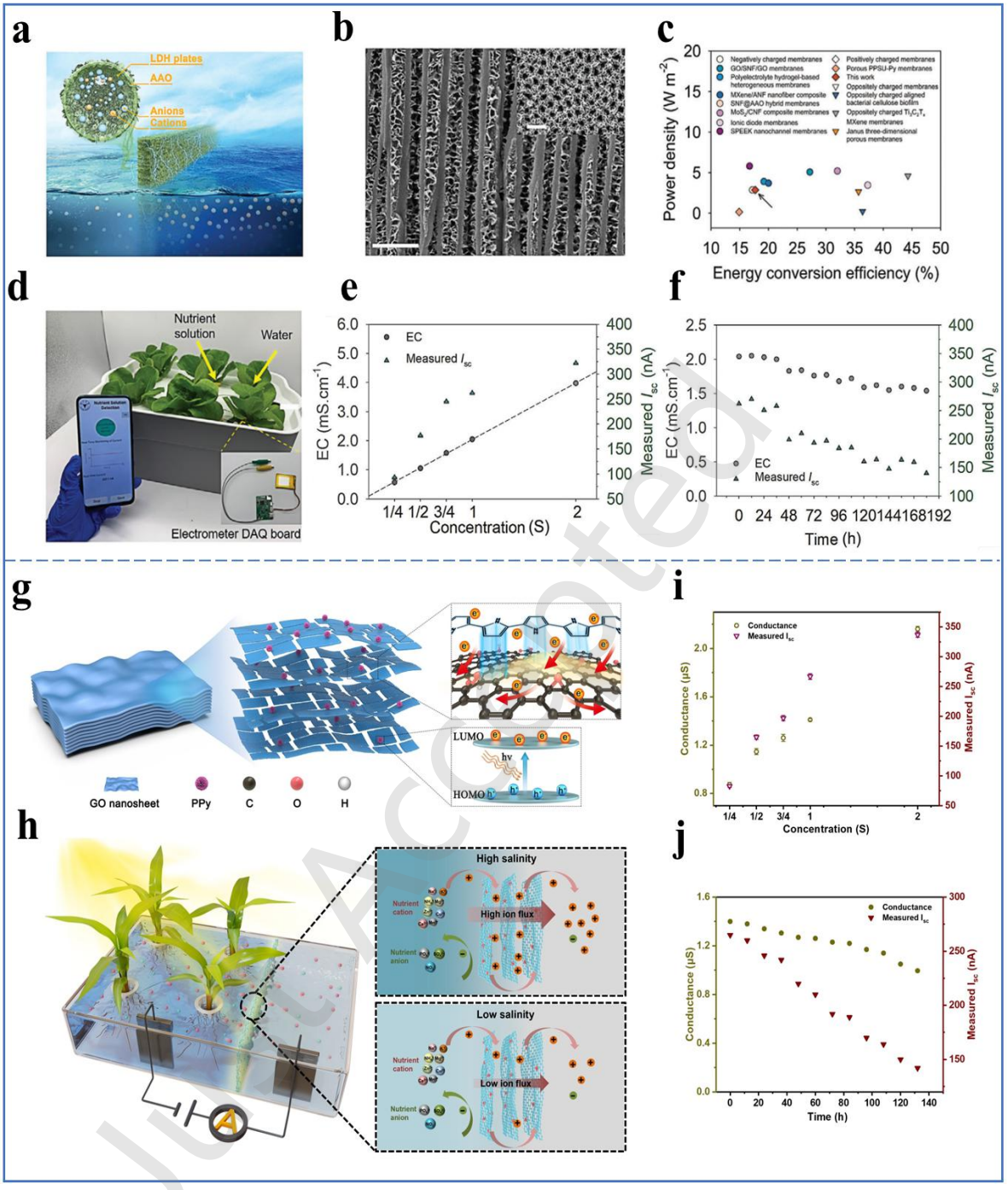

Figure 5. (a) Schematic illustration of osmotic power generation and anion-selective transport of the LDH@AAO composite membrane. (b) Cross-sectional SEM image of the LDH@AAO composite membrane. (c) Performance comparison of the LDH@AAO composite membrane with reported nanofluidic membranes. (d) Photograph of the self-powered real-time nutrient solution detection system based on the LDH@AAO composite membrane. (e) Measured short-circuit current and electrical conductivity corresponding to different nutrient solution concentrations. (f) Variation of measured short-circuit current and EC during 7-day monitoring of romaine lettuce hydroponic cultivation. (Reproduced with permission from Ref. [69], Copyright 2022, Wiley-VCH Verlag.) (g) Schematic illustration of the PyGO heterochannels under light irradiation. (h) Schematic diagram of the sunlight-amplified self-powered real-time system based on the PyGO membrane. (i) Measured short-circuit current and ionic conductance under light irradiation corresponding to different nutrient solution concentrations. (j) Dynamic variation of measured short-circuit current and ionic conductance under light irradiation during hydroponic cultivation monitoring. (Reproduced with permission from Ref. [87], Copyright 2022, Wiley-VCH Verlag.)

current closely matched the changes in nutrient solution conductivity, demonstrating that the system can accurately track dynamic changes in nutrient concentration. Although the membrane experienced a slight performance decay of

12.8% after prolonged immersion, it still maintained stable signal output, highlighting its potential for in-situ agricultural monitoring applications.

Apart from the nutrient sensing enabled by anion-selective membranes, more widely present cation-selective membranes can also be used to detect nutrients in hydroponic agriculture. Apart from the nutrient sensing enabled by anion-selective membranes, more widely present cation-selective membranes can also be used to detect nutrients in hydroponic agriculture. Guo et al. [87] fabricated a free-standing polypyrrole-GO (PyGO) lamellar conductive heterochannel membrane via a facile super-assembly strategy, which possessed tailored channel-sized gradients and inherent optical-electrical coupling sensitivity. As schematically illustrated in Figure 5g, negatively charged PyGO heterochannels repel anions through electrostatic repulsion and enable efficient cation-selective transport driven by salinity gradients; under light illumination, efficient separation of photogenerated carriers in PPy and GO further enhances surface negative charge density and electric double-layer overlap, thus remarkably promoting cation-selective transmembrane transport. Benefiting from the distinctive optical-electrical coupling property, a sunlight-amplified self-powered nutrient detection system was constructed based on the cation-selective PyGO membrane for real-time hydroponic monitoring, as displayed in Figure 5h. Similar to the anion-selective sensing system, this fully integrated device belongs to a typical self-powered sensor, in which the cation-selective nanofluidic membrane undertakes both osmotic energy conversion and nutrient concentration sensing simultaneously, fully complying with the integrated design principle. As depicted in Figure 5i, the short-circuit current and ionic conductance measured under light illumination show a significant positive correlation with nutrient solution concentration, which can be directly adopted as sensitive indicators for quantitative ion concentration detection. During long-term in-situ monitoring of hydroponic cultivation (Figure 5j), the short-circuit current and conductance signals under light illumination decrease gradually with the consumption of nutrients in the solution, and the variation trends of electrical signals are highly consistent with the dynamic change of nutrient concentration.

Notably, the short-circuit current and conductance values obtained under illumination are considerably higher than those measured in the dark state, presenting an obvious light-induced enhancement in sensing signals and detection sensitivity. The membrane maintains stable signal output with only slight performance decay after continuous operation, demonstrating its favorable long-term stability for in-situ agricultural monitoring. This optical-electrical coupled cation-selective system introduces light regulation into self-powered nutrient sensing. With high cation selectivity, light-enhanced ion transport, and stable sensing performance, the PyGO heterochannel membrane provides a novel and efficient strategy for real-time and in-situ nutrient monitoring in smart hydroponic agricultural systems.

3.2 Pressure sensing enabled by 2D GO Composite

Inspired by the ion concentration gradient-driven mechanoreceptors in human skin biosensing systems, ion electronic pressure sensors based on 2D nanofluidic effects have emerged as a key direction for the direct utilization of osmotic energy. By mechanically tuning the interlayer spacing of 2D materials to precisely control ion selective migration, osmotic energy is directly converted into encodable electrical signals, providing a novel paradigm for constructing self-powered pressure sensing systems. This approach also opens new pathways for the direct application of osmotic energy in practical scenarios.

To achieve the direct and efficient utilization of osmotic energy, Yu et al. [81] constructed a flexible all-solid-state 2D nanofluidic pressure sensor powered by osmotic energy, with a nanofluidic membrane made from KOH-modified GO (KGO) and pristine GO serving as its functional component (Figure 6a). The surface of GO is rich in oxygen-containing functional groups such as -OH and -COOH, giving it high electronegativity and imparting cation selectivity. After KOH modification, KGO and GO form a stable built-in ion concentration gradient. Specifically, DFT calculations confirm that the adsorption energy of K^+ on GO is much higher than that of OH^- (Figure 6b), indicating that K^+ can be more stably adsorbed onto the GO surface, with a low migration barrier of 0.20 eV. In contrast, OH^- experiences a

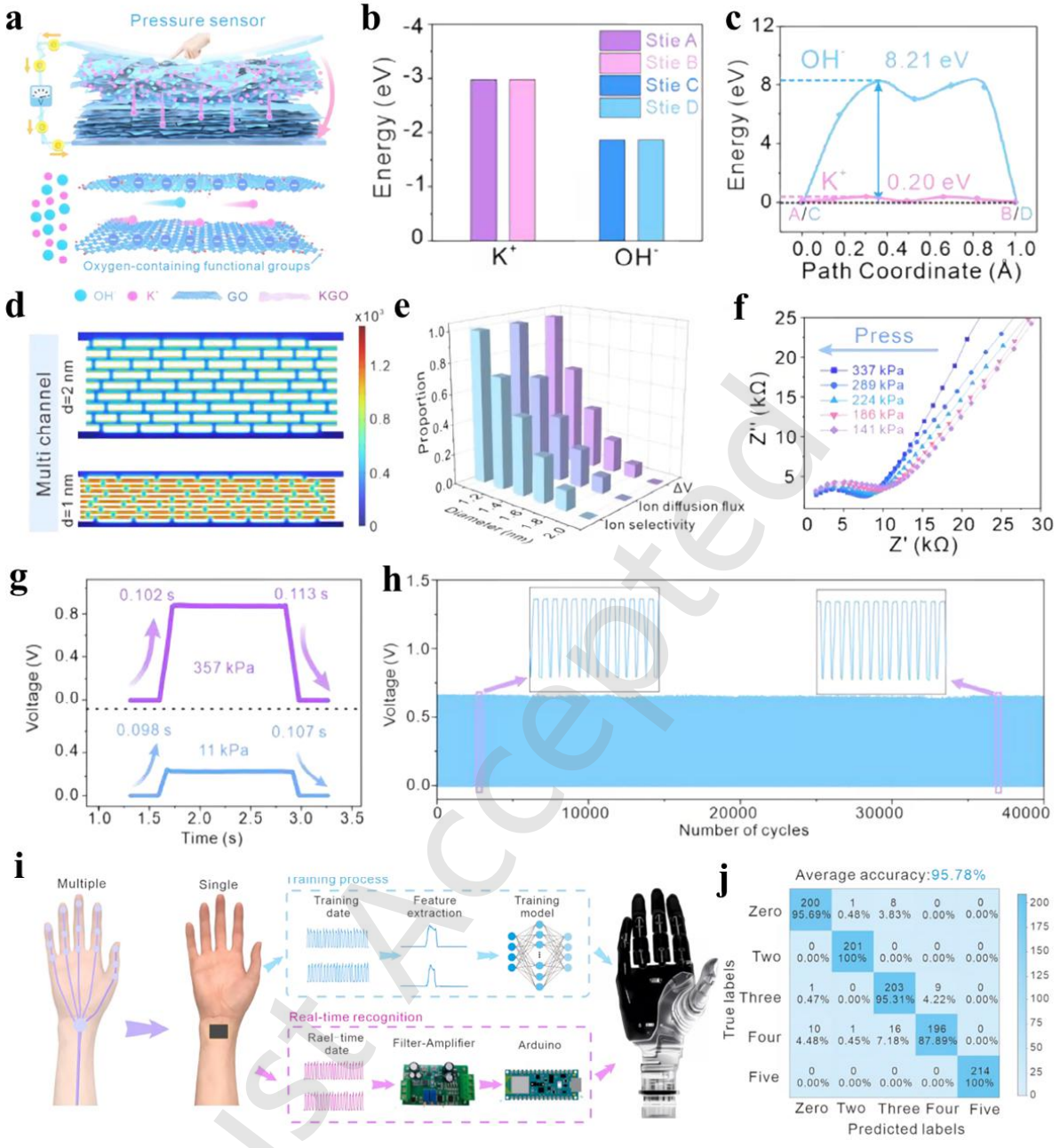

Figure 6. (a) Schematic diagram of the flexible all-solid-state 2D nanofluidic pressure sensor based on KGO and GO nanofluidic membrane. (b) Adsorption energies of K^+ and OH^- on the GO surface from DFT calculations. (c) Migration barrier of K^+ and OH^- on the GO surface from DFT calculations. (d) Cation distribution in the vertical nanochannel with the channel size compressed from 2 to 1 nm. (e) Variations of cation selectivity, diffusion flux and membrane potential difference with the nanochannel size. (f) Electrochemical impedance spectroscopy of the pressure sensor during the pressing process. (g) Response and recovery time of the pressure sensor under different pressure stimuli. (h) Cycling stability test of the pressure sensor. (i) Schematic illustration of the training and real-time recognition process of the human-machine interaction system. (j) Confusion matrix of gesture recognition for five gestures. (Reproduced with permission from Ref. [81], Copyright 2025 Wiley-VCH Verlag.)

high migration barrier of 8.21 eV due to electrostatic repulsion (Figure 6c). This allows for the directional and rapid adsorption and migration of K^+ while effectively repelling anions, forming stable ion-selective characteristics within the nanochannels. In 2D GO nanofluidic channels, K^+ transport follows two distinct patterns: in-layer diffusion inside single-layer nanosheets and interlayer diffusion between adjacent nanosheets. In-layer diffusion shows a low and steady energy barrier that is hardly affected by interlayer distance. By comparison, interlayer diffusion possesses a much higher energy barrier and is more sensitive to the change of interlayer spacing. As the

interlayer channel becomes narrower, the interlayer diffusion barrier decreases significantly. Thus, the interlayer diffusion serving as the rate-determining step that dominates the pressure-sensing behavior. Upon applying pressure to the sensor, the interlayer spacing of the 2D materials compresses (Figure 6d), enhancing the EDL overlap effect within the nanochannels. This increases cation selectivity, diffusion flux, and the potential difference across the membrane (Figure 6e). Consequently, the device resistance decreases as the interlayer spacing reduces, leading to an increase in the open-circuit voltage and direct conversion of pressure into electrical signals (Figure 6f). After geometric optimization, the sensor demonstrates excellent performance with a response/recovery time as low as 115.0/128.0 ms (Figure 6g). After 40,000 pressure cycles, the electrical signal only experiences a 5% loss, indicating strong stability of the pressure sensor (Figure 6h). When 12 units are stacked vertically, the output voltage reaches up to 13.10 V, with a pressure detection range extending to 360 kPa. The sensor can be integrated with deep learning algorithms (Figure 6i) to capture minute fluctuations of the human wrist tendon, achieving an impressive recognition accuracy of 95.78% for five hand gestures (Figure 6j). This successful practical utilization enables high-resolution human-machine interaction and addresses the redundancy issue associated with traditional multi-sensor systems.

3.3 Humidity sensing enabled by 3D HOFs

The key challenge of self-powered humidity sensing lies in realizing efficient energy conversion and high-performance humidity response simultaneously, which requires the rational integration of osmotic energy conversion mechanisms and humidity-responsive ion transport behavior. Traditional self-powered humidity sensors are limited by the single ion transport path and weak environmental responsiveness of electrolytes, leading to low energy conversion efficiency and slow humidity response speed, which severely restricts their practical application in flexible wearable and non-contact sensing. In contrast, HOF-based electrolytes with Na^+ concentration gradient design break through the above limitations by virtue of their reversible humidity-responsive ion migration barrier regulation and excellent cation selective transport properties, enabling the efficient conversion of humidity gradient into electrical signals and thus becoming a promising candidate for high-performance self-powered humidity sensing.

Chen et al. [117] fabricated a flexible self-powered MHCNM humidity sensor with a built-in concentration gradient by employing MXene as symmetric electrodes and HOF/CNF and HOF/CNF/NaCl as dual electrolytes (Figure 7a). Energy-dispersive spectroscopy (EDS) characterization of the two electrolytes confirmed the uniform distribution of C and O elements in the HOF/CNF electrolyte (Figure 7b), as well as the homogeneous dispersion of C, O, Na, and Cl elements in the HOF/CNF/NaCl electrolyte (Figure 7c), which not only ensures the uniform loading of electrolyte components but also establishes a structural foundation for the stable construction of a Na^+ concentration gradient between the two electrolytes and for the subsequent uniform ion transport. To optimize electrolyte performance, this work fabricated the HOF/CNF nanochannel membrane by compositing HOF-H4TCPB with CNF. Such modification overcomes the brittleness of the pure HOF-H4TCPB membrane while endowing the composite membrane with a negatively charged surface (zeta potential of approximately −48.8 mV, Figure 7d), which indicates that the nanochannel surface is negatively charged due to the presence of unprotonated carboxyl groups, and excellent hydrophilicity (contact angle of 27.5°, Figure 7e), creating favorable conditions for selective Na^+ transport and water molecule adsorption. The humidity sensing mechanism is based on the reversible regulation of the Na^+ migration energy barrier within the HOF nanochannels by environmental water molecules, which play multiple physicochemical roles during this process (Figure 7f). Specifically, under low-humidity conditions, the lack of water molecules maintains a high migration energy barrier for Na^+, and NaCl in the solid-state electrolyte cannot dissociate into free ions, thereby hindering the directional migration of Na^+ along the concentration gradient; under high-humidity conditions, the hydrophilic HOF/CNF membrane absorbs a large number of water molecules, which not only effectively lower the Na^+ migration energy barrier within the nanochannels but also act as a solvent to dissociate NaCl into hydrated sodium and chloride ions capable of moving freely within the channels, while the accumulation of water molecules in the

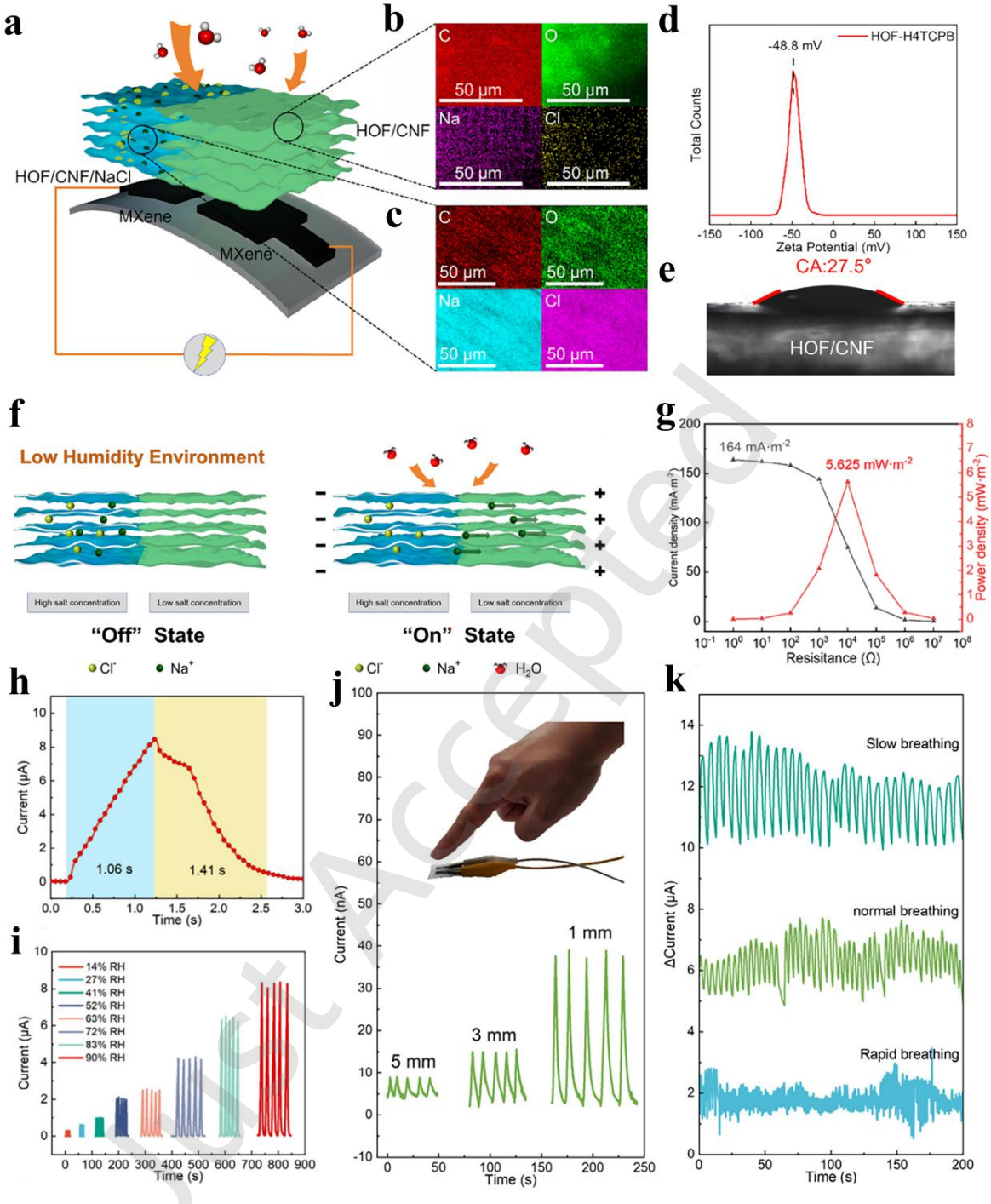

Figure 7. (a) Schematic diagram of the MHCNM humidity sensor structure. (b) EDS images of C and O distribution in HOF/CNF electrolyte. (c) EDS images of C, O, Na and Cl distribution in HOF/CNF/NaCl electrolyte. (d) Zeta potential of HOF-H4TCPB. (e) Contact angle of HOF/CNF composite membrane. (f) Schematic illustration of ion transport mechanism of MHCNM humidity sensor in on/off states. (g) Current density and power density of MHCNM humidity sensor. (h) Response/recovery time of the sensor. (i) Dynamic current response of MHCNM humidity sensor at 11-95% RH. (j) Non-contact sensing performance of the sensor. (k) Respiratory detection performance of the sensor. (Reproduced with permission from Ref. [117], Copyright 2025, Wiley-VCH Verlag.)

hydrophilic pores forms continuous ion transport pathways that promote high ion flux and drive efficient directional migration of Na^+ from the high-concentration side to the low-concentration side of the electrolyte. The negatively charged nanochannels strongly repel Cl^-, suppressing their concurrent migration and thereby generating a stable potential difference across the electrolyte membrane, converting humidity variations into a stable electrical signal

and achieving a high current density of 164 $mA \cdot m^{-2}$ and a power density of 5.625 $mW \cdot m^{-2}$ (Figure 7g). The MHCNM sensor exhibits excellent humidity sensing performance, with a response time as low as 1.06 s and a recovery time of only 1.41 s (Figure 7h). Its dynamic response curves over a relative humidity range of 11%-95% further confirm the wide humidity response range and high sensitivity of the sensor, with the current signal continuously increasing as humidity rises (Figure 7i). After more than 200 humidity cycles, the sensor still maintains stable electrical signal output, demonstrating outstanding sensing stability. In practical sensing applications, the device enables non-contact monitoring of human skin humidity, producing distinct current response signals at distances of 1 mm, 3 mm, and 5 mm from a human finger (Figure 7j), and can accurately capture dynamic changes in human respiration, clearly distinguishing slow, normal, and rapid breathing patterns by characteristic frequency (Figure 7k), highlighting its significant potential in flexible wearable electronics, intelligent non-contact sensing, and medical diagnostics.

3.4 Image sensing enabled by 2D GO nanosheets

The evolution of image sensors has laid a core foundation for the advancement of modern visual perception systems [118-120]. From early analog photosensitive devices to the current high-pixel, high-frame-rate intelligent imaging modules, it has realized the leaping development of image capture and signal processing technologies [121, 122]. With the ever-rising demands for imaging precision, response speed and scene adaptability in diverse fields such as consumer electronics, industrial inspection, biomedicine and security monitoring, image sensors have become an indispensable core component of various visual systems [123, 124], and their technological innovation is constantly advancing toward the directions of low power consumption, miniaturization and self-powering. Osmotic energy-driven self-powered ionic image sensing technology is precisely an important research direction under this development trend. A core bottleneck in osmotic energy-driven self-powered ionic image sensing is achieving efficient optical-to-ionic signal transduction and high-density device integration without external power supply. Conventional ionic sensing systems often fail to balance response sensitivity and practical applicability due to low single-channel transport efficiency and poor consistency after integration. Photoresponsive highly aligned nanochannels (pHANCs) offer a novel solution to this dilemma through the synergistic effect of ordered structure and light-responsive regulation.

Huang et al. [125] developed a pHANCs-based biomimetic photoreceptor array, establishing the core architecture of an osmotic energy-powered ionic imaging sensor (Figure 8a). In this design, photoacid molecules were noncovalently grafted onto graphene oxide nanosheets, and after ordered stacking, the interlayer spacing was expanded from 0.86 nm to 1.09 nm, directly reducing ionic hydrodynamic resistance and markedly enhancing ionic conductivity compared with the pristine system, thereby providing a structural foundation for efficient ion transport. The response mechanism of the sensor relies on light-regulated modulation of the entrance energy barrier. Under dark conditions, cations accumulate within the negatively charged nanochannels, and ion transport is governed by the entrance barrier (Figure 8b). Upon light irradiation, the photoacid molecules release protons and increase the surface charge density of the channels (Figure 8c), while the variation of ionic conductivity with the reciprocal of temperature exhibits typical Arrhenius behavior, and the entrance energy barrier for cation transport decreases from 0.21 eV to 0.176 eV (Figure 8d), ultimately resulting in an ionic current response three times higher than that in the dark state. In addition, after light irradiation, the contact angle of the pHANCs decreases from 21° to 16°, indicating significantly enhanced hydrophilicity, which further facilitates electrolyte infiltration and ion migration. On this mechanism basis, an 8 × 8 biomimetic photoreceptor array, integrated with a flexible layered structure based on a PET substrate (Figure 8e), was successfully developed into an imaging sensor that precisely accomplished digital decoding of incident light patterns through current ratio differences among individual units (Figure 8f). The device maintained stable performance after repeated bending and successfully achieved accurate recognition of numerical patterns from 0 to 9, laying an important foundation for the practical implementation of wearable self-powered visual sensing technologies. Notably, a single photoreceptor exhibited outstanding performance,

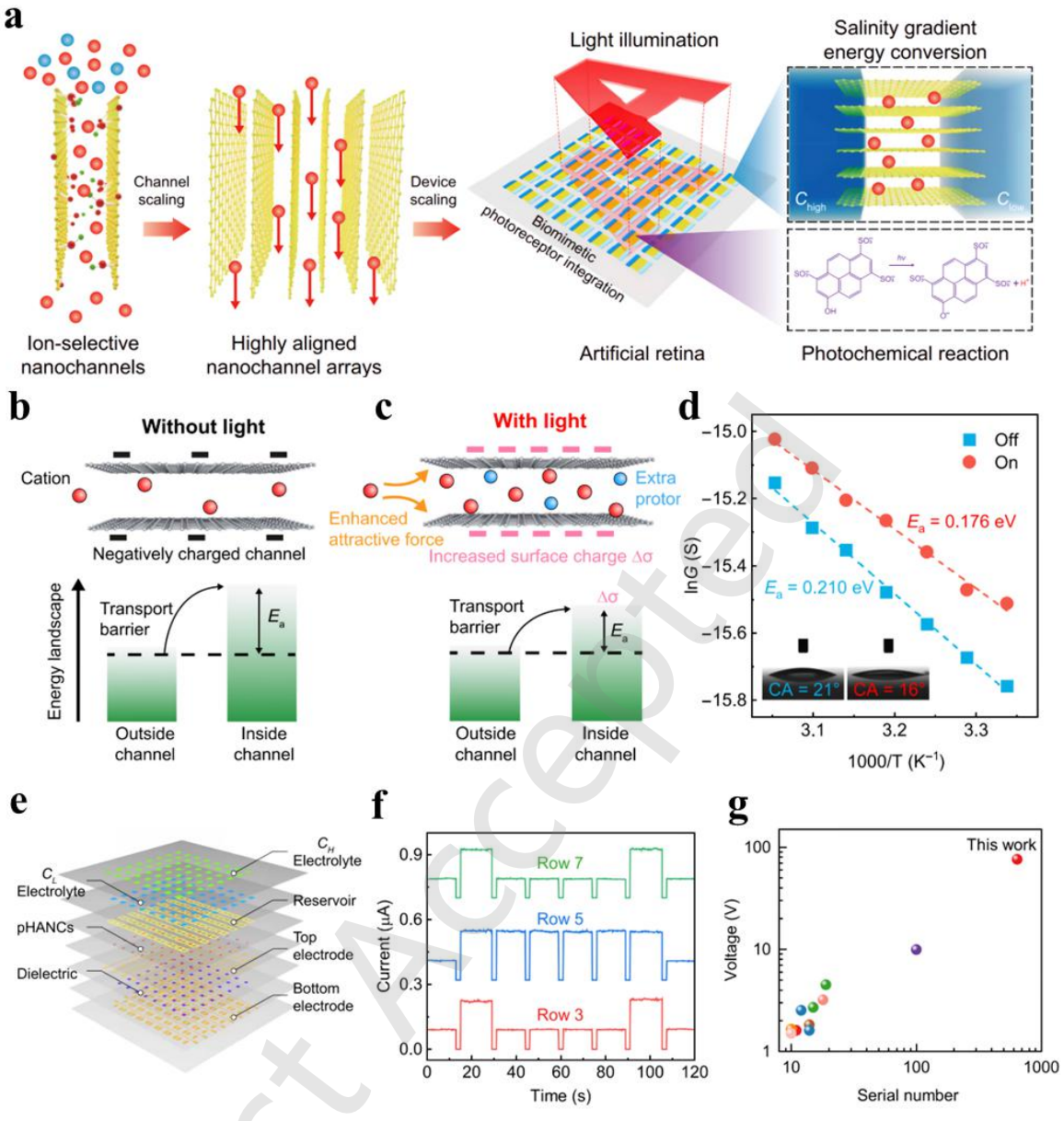

Figure 8. (a) Schematic illustration of the biomimetic photoreceptor array architecture based on pHANCs for self-powered ionic image sensing (b) Schematic of ion transport through pHANCs under dark conditions. (c) Schematic of ion transport through pHANCs under light irradiation (d) Arrhenius behavior of ionic conductivity for pHANCs, with the inset showing the contact angle change upon illumination. (e) Layered structure schematic of the flexible PET-based device for ionic image sensing. (f) Digital decoding of incident light patterns via current ratio differences in the 8×8 photoreceptor array. (g) Integration performance of serially connected pHANC photoreceptors, demonstrating the record output voltage and scale. (Reproduced with permission from Ref. [125], Copyright 2024, American Association for the Advancement of Science.)

delivering a power density of 148.3 $W \cdot m^{-2}$ under 405 nm illumination, comprehensively surpassing previously reported membrane-based osmotic systems; after series connection of 640 units, the output voltage exceeded 76 V, setting new records in both integration scale and output performance (Figure 8g).

In summary, multiple concentration gradient construction strategies have been developed for osmotic energy- driven self- powered sensing, including external environment- dependent gradients and various built- in concentration gradients. The above research represents three divergent trajectories: realizing nutrient sensing by virtue of extrinsic concentration gradients, achieving pressure and humidity sensing through built-in gradients within the membrane, and accomplishing image sensing by constructing built-in gradients inside the sensor but outside the membrane. Compared with extrinsic gradients, built-in gradients completely break away from the dependence on

the ionic concentration distribution of the external environment and enable the autonomous construction of stable ionic concentration differences. This not only greatly enhances the environmental adaptability and scenario compatibility of the sensing system, effectively avoids the instability of sensing signals caused by the dynamic fluctuation of environmental gradients and ensures detection accuracy and long-term operational reliability, but also is highly suitable for the application requirements of flexible wearable sensing due to the flexibility and integration of structural design, emerging as a strong competitor for the next-generation intelligent sensing technology. In contrast to the built-in gradients inside the sensor but outside the membrane, the built-in gradients within the membrane realize the deep coupling of ion transport and gradient regulation in the core sensing membrane layer, which greatly reduces energy loss during gradient transmission and significantly improves the efficiency and response speed of signal transduction. Meanwhile, it makes the device structure more compact, further strengthening the application advantages of flexible and miniaturized sensing.

4. Other emerging applications

Beyond osmotic energy-driven self-powered sensing, recent studies have also witnessed emerging breakthroughs of self-powered lithium extraction and self-powered hydrogen production driven by osmotic energy. As highly promising extensions of osmotic energy utilization, both applications are in an early and highly emerging stage. Although numerous advances have been achieved in functional membranes on osmotic energy harvesting and ion-selective transport, their practical implementation toward efficient, stable, and scalable lithium extraction and hydrogen production systems remains challenging. In the following sections, we summarize the currently developed technical routes, analyze their inherent advantages and existing bottlenecks, and aim to provide meaningful guidance for the future exploration of more diversified osmotic energy self-powered applications.

4.1 Osmotic energy-driven self-powered lithium extraction

With the acceleration of global electrification lithium-ion batteries are increasingly used in portable electronic devices electric vehicles and renewable energy storage systems highlighting the strategic importance of lithium resources [126-128]. Global lithium production has more than tripled over the past decade and multiple studies predict that lithium demand will triple again in the next decade [129, 130]. Conventional lithium reserves are limited and are expected to be depleted by 2080 [131, 132]. Therefore, developing efficient extraction technologies for unconventional lithium sources such as oil-produced water geothermal brines and Dead Sea brines has become crucial to ensuring the stability of the lithium supply chain [133-135]. Against this backdrop, direct lithium extraction technologies have emerged rapidly due to their high efficiency flexibility and environmental compatibility. Among them, osmotic energy self-powered lithium extraction technology by capturing the intrinsic osmotic energy in ion separation processes achieves the synergy of lithium extraction and energy utilization offering a new path for low-energy-consumption lithium recovery.

However, traditional unconventional lithium extraction technologies have numerous drawbacks that hinder their practical application. Evaporation methods are not only time-consuming and wasteful of water resources but also unsuitable for low-lithium brines [136, 137]. Chemical precipitation methods involve toxic chemicals leading to environmental pollution [138, 139]. Traditional membrane-based lithium extraction technologies such as electrodialysis and nanofiltration although offering certain selectivity, require substantial external electrical input and suffer from high thermodynamic potentials and overpotentials [134, 135, 140, 141]. More critically, membrane technology has an inherent weakness, fouling. Preventing fouling requires expensive brine pretreatment, which may completely offset the benefits of osmotic energy harvesting [142]. Additionally traditional electrochemical lithium extraction technologies often suffer from ion back mixing due to poor membrane selectivity or limited throughput due to the cumbersome post-treatment required for adsorbent regeneration [143, 144]. These limitations have driven the development of novel lithium extraction technologies such as membrane-free decoupling and in-situ

osmotic energy utilization.

Osmotic energy is inherently present in lithium extraction devices and the entire separation process. Its utilization requires no additional auxiliary equipment and can be perfectly integrated into electrochemical electrolysis systems featuring excellent integration and device unity making it the most direct pathway for coupling osmotic energy utilization with electrolytic lithium extraction. However traditional membrane-based lithium extraction technologies have failed to tap into this intrinsic energy and even require massive external electrical input for ion migration, resulting in low energy utilization efficiency and poor process integration. In recent years, two representative technical routes have been developed to realize in-situ harvesting and utilization of osmotic energy in lithium extraction systems, achieving the synergy of lithium separation and energy output/consumption reduction. Therefore, the in-situ integration of osmotic energy harvesting into lithium extraction electrolysis systems presents a promising avenue for the development of high-integration energy-saving lithium recovery technologies.

The first technical route is the membrane-based spontaneous lithium extraction system developed by Zhang et al. [145] which achieves net energy output by coupling Li-selective ceramic membranes with Cl^--storing electrode pairs. The self-powered mechanism with net energy output originates from the huge Cl^- concentration gradient between the feeding brine and receiving solution (Figure 9a). This gradient generates abundant osmotic energy forming an electrochemical potential difference consisting of membrane potential and electrode potential. Closing the external circuit drives electrons to flow spontaneously from the Ag electrode to the AgCl electrode forming a continuous electron current for direct net energy output. Meanwhile Li^+ migrates through the Li-selective membrane to balance the charge of Cl^- stored/released by the electrodes realizing spontaneous Li extraction without external energy input. The Li-selective membrane adopts NASICON-type $Li_{1.5}Al_{0.5}Ge_{1.5}(PO4)_3$ (LAGP) ceramic whose crystal structure features triangular transport bottlenecks with a diameter of less than 1.8 Å (Figure 9b). Dehydrated Li^+ (1.2 Å) can pass through these bottlenecks freely while Na^+ (1.9 Å) is blocked by size effects and Mg^{2+} is hindered by ultrahigh dehydration free energy. XRD patterns confirm that the LAGP membrane maintains structural stability after 300 hours of operation ensuring sustained selective performance. This highly integrated system exhibits excellent lithium extraction performance with net energy output. Using 0.5 M $MgCl_2$ and 0.03 M LiCl as the feed, it achieves stable operation for over 300 hours after 15 electrode switches, maintaining a near-unity Faraday efficiency of ~100% (Figure 9c) and an ultrahigh Li/Mg molar selectivity of 450 with Mg^{2+} leakage of less than 4% (Figure 9d). The average net energy output reaches 1.6 $Wh \cdot mol_{Li}^{-1}$ and it even realizes 10-fold spontaneous Li^+ enrichment in brine with a Mg/Li molar ratio of 1667 while outputting energy. Figure 9e further confirms that this lithium extraction is fully self-powered and can also be utilized to power external devices, in sharply contrast with conventional systems. However, this system has an operational limitation: continuous lithium extraction relies on repeated electrode switching after the Ag/AgCl electrode pair is exhausted, which brings practical inconvenience for large-scale application. Moreover, the discharge voltage gradually declines with each electrode switch, as the Cl^- concentration gradient between the feed and receiving solution dissipates progressively during lithium migration, weakening the electrochemical driving force. Fortunately, these issues are not insurmountable and can be effectively addressed by engineering optimizations, such as adopting a stacked device configuration with anion exchange membranes to enable continuous operation without electrode switching, and implementing continuous feed supplementation and effluent separation to maintain a stable Cl^- concentration gradient.

Inspired by the concept of decoupled electrolysis, Li et al. [146] have developed a membrane-free technical route that eliminates the need for separation membranes thus fundamentally addressing the problems of membrane fouling and excessive pretreatment costs. This decoupled membrane-free (DCMF) electrochemical system enables harvesting the electrical potential energy inherent in the concentration gradient between brine and receiving solution without any separation membrane. The self-powered auxiliary mechanism of this membrane-free system originates from the concentration gradient of halide anions

(Cl^-/Br^-) between the brine and extraction solution (Figure 9f). Based on the Nernst equation of Ag/AgX electrodes this gradient generates an osmotic potential (Figure 9g) which acts as an internal power source (Figure 9h) reducing the external energy demand for lithium extraction. The $FePO_4/LiFePO_4$ electrodes serve as the core selective

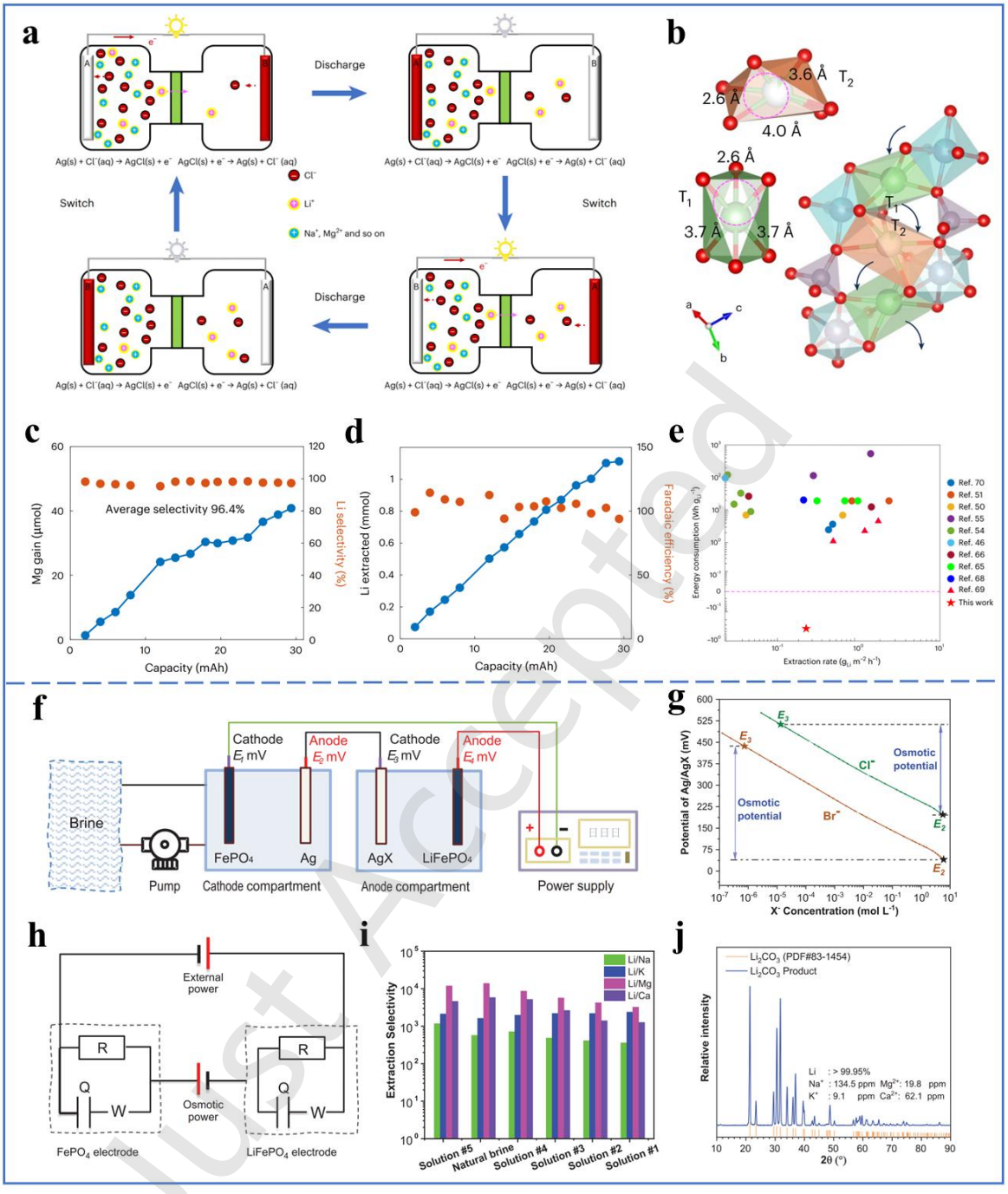

Figure 9. (a) Schematic illustration of the spontaneous lithium extraction system based on Li-selective LAGP membrane and Ag/AgCl electrode pair. (b) Crystal structure of NASICON-type LAGP ceramic with triangular Li^+ transport bottlenecks. (c) Faradaic efficiency and amount of extracted Li versus discharge capacity. (d) Mg^{2+} leakage and Li/Mg molar selectivity versus discharge capacity. (e) Energy consumption and extraction rate of this spontaneous method with other methods. (Reproduced with permission from Ref. [145] Copyright 2024, Springer Nature.) (f) Schematic illustration of the DCMF electrochemical lithium extraction system. (g) Theoretical dependence of the Ag/AgX electrode potential on the halide anion (Cl^-/Br^-) concentration. (h) Equivalent circuit diagram of the DCMF system, where the osmotic potential acts as an internal power source. (i) Li/Mg extraction selectivity of the DCMF system for brines with different Mg/Li molar ratios. (j) X-ray diffraction (XRD) pattern and elemental analysis results of the produced battery-grade Li_2CO_3 (Reproduced with permission from Ref. [146],Copyright 2024, American Association for the Advancement of Science.)

components. Li^+ is preferentially intercalated into the $FePO_4$ framework due to its higher intercalation potential compared to Na^+, K^+, Mg^{2+} and Ca^{2+} while other cations are effectively excluded. The Ag/AgX electrodes mediate the

transfer of halide anions maintaining charge balance across the physically isolated cathode (brine) and anode (extraction solution) compartments. This membrane-free design ensures stable long-term operation. The system exhibits excellent lithium extraction performance. When treating brines with Mg/Li molar ratios up to 3258 and Li^+ concentrations as low as 0.71 mM it achieves Li/Mg selectivities of 3247-11987 (Figure 9i) and near-unity coulombic efficiency (>99%) over 1000 cycles. A pilot-scale system with a 33.75 m^2 electrode area realizes 84.0% lithium recovery from Dead Sea brine producing battery-grade Li_2CO_3 (>99.95% purity) with 21.5% energy savings via osmotic energy harvesting (Figure 9j). However the DCMF system has inherent limitations. The osmotic energy harvesting efficiency is relatively low with the harvested osmotic energy accounting for only 3.48% of the direct lithium extraction energy consumption in the pilot-scale test. It cannot achieve fully osmotic energy-driven self-powered lithium extraction and still relies on external power supply as the main energy source. Meanwhile the membrane-based system faces challenges in stability in Na-rich brines and relatively high material costs.

These studies yield crucial insights for osmotic energy utilization and ion separation. Osmotic energy can be harvested for lithium extraction without separation membranes, as realized in the DCMF system via Ag/AgX redox electrodes that respond to halide anion (Cl^-/Br^-) concentration gradients between brine and extraction solution. Following the Nernst equation, the gradient generates a spontaneous osmotic potential on Ag/AgX electrodes, which acts as an internal power source to drive charge transfer. Essentially, this osmotic energy is the chemical potential energy derived from the halide anion concentration difference across the physically isolated compartments. Moreover, ion selectivity is not only achievable via electric field regulation but also can be realized through the size-sieving effect of nanochannels in solid membranes. These findings broaden the design ideas for osmotic energy-driven ion separation technologies, providing new directions for developing more flexible, diverse and efficient separation systems for resource recovery from complex aqueous solutions.

In summary, osmotic energy-driven self-powered lithium extraction is still in an emerging and initial research stage, and the reported technical schemes have certain inherent limitations to be addressed. Besides the aforementioned operational inconveniences, voltage decay, low osmotic energy utilization efficiency and material cost issues, the technology also faces challenges such as insufficient scalability and stability in complex brine systems for practical industrial application. Nevertheless, these routes possess irreplaceable advantages that traditional lithium extraction technologies cannot match: they realize lithium extraction with net energy output or significant energy saving by harvesting intrinsic osmotic energy from brines, break the energy consumption logic of conventional methods, and achieve ultrahigh Li/Mg selectivity with simple processes and low environmental impact. These unique merits make osmotic energy-driven self-powered lithium extraction a promising alternative for sustainable lithium production, with broad development potential in the future.

4.2 Osmotic energy-driven self-powered hydrogen production

Driven by the global goal of carbon neutrality, hydrogen energy has become a pivotal carrier in the decarbonized energy system due to its ultra-high gravimetric energy density [147], zero-carbon combustion byproducts [148], and renewable nature [149], showing broad application prospects in power, transportation, and other fields [150]. However, current hydrogen production remains highly dependent on fossil fuels [151], resulting in significant greenhouse gas emissions [152]. Although traditional water electrolysis technology can produce high-purity hydrogen, it faces bottlenecks such as high-power consumption and reliance on external power grids [153-155]. Furthermore, renewable energy sources like wind and solar power suffer from geographical limitations and seasonal fluctuations [155, 156], which further restrict the large-scale application of green hydrogen. Electrochemical water splitting, the core technology for green hydrogen production, relies on two key electrochemical reactions under alkaline conditions: the hydrogen evolution reaction (HER: $2H_2O + 2e^- \rightarrow H_2 + 2OH^-$) at the cathode and the oxygen evolution reaction (OER: $4OH^- \rightarrow 2H_2O + O_2 + 4e^-$) at the anode. Despite advances in catalyst

design and electrolyzer optimization to reduce overpotentials, the OER involves a four-electron transfer process with slow kinetics, requiring continuous, stable, and environmentally friendly electrical input [157, 158]. Most current research focuses on improving catalytic activity and electrolyzer efficiency, while harnessing natural renewable energy to directly drive water electrolysis for self-powered hydrogen production without external power supply has emerged as an important direction with both academic value and application prospects, offering new ideas to break the power dependence bottleneck in large-scale green hydrogen applications [159-163].

Osmotic energy derived from the salinity gradient at the seawater-river water interface has become an ideal energy source for self-powered hydrogen production due to its abundant reserves, stable output, and independence from weather and seasons. It is estimated that the theoretical global reserve of osmotic energy at the seawater-freshwater interface reaches 30 terawatts, showing enormous development potential. The collection and conversion of osmotic energy mainly rely on RED devices, whose core is to convert the chemical potential difference generated by the salinity gradient into electrical energy through the selective ion transport of ion-selective membranes, thereby powering water electrolysis for hydrogen production. Compared with traditional hydrogen production technologies, osmotic energy-driven self-powered hydrogen production requires no additional energy input, enabling direct conversion from "blue energy to electrical energy to hydrogen energy". It not only reduces carbon emissions but also efficiently utilizes the natural energy endowments of oceans and rivers, opening up a sustainable new pathway for green hydrogen production. However, conventional ion-selective membranes suffer from limitations such as insufficient ion selectivity, poor mechanical robustness, and difficulties in large-scale fabrication, hindering the practical implementation of salinity gradient-powered water electrolysis for hydrogen production. To address these challenges, researchers have conducted a series of studies on the design and synthesis of high-performance ion-selective membranes and device integration optimization. Among them, the works of He et al. [164] and Liang et al. [165] have achieved breakthrough progress in large-scale fabrication and complex environmental adaptability, respectively, providing important support for the development of this technology.

He et al. [164] developed a precisely designed polyamic acid (PAA37) ion-selective membrane, realizing the integration of ultra-high cation selectivity and large-area scalable preparation. Combined with an optimized module assembly strategy, they constructed an integrated self-powered hydrogen production device, breaking the scalability bottleneck of osmotic energy harvesting for hydrogen production and opening up a new practical pathway for blue energy utilization and green hydrogen synthesis. The integrated self-powered hydrogen production device is composed of PAA37-based osmotic energy power modules (OEPMs) connected in series with an electrocatalytic water electrolysis unit, where the OEPMs convert salinity gradient energy into electrical energy through cation-selective directional ion transport. The core material of the device is the PAA37 membrane, which is synthesized via a one-step polycondensation reaction of pyromellitic dianhydride and 1,4-bis(4-aminophenoxy) benzene (Figure 10a). The ultra-high cation selectivity of the membrane originates from the synergistic effect between high-density carboxylic acid groups and sub-nanometer channels with a central pore size of approximately 9 Å (Figure 10b): the negatively charged carboxylic acid groups enable preferential adsorption of cations and repulsion of anions, while the confinement effect of the sub-nanometer channels further enhances the electrostatic interaction between ions and the channel walls. Ultimately, the membrane achieves a cation transference number of 0.96, approaching the ideal value, and this excellent selectivity also guarantees the high Faraday efficiency of the subsequent hydrogen evolution reaction. The team also realized the large-area preparation of the PAA37 membrane via a roll-to-roll method, with the membrane area reaching up to 9000 cm^2, and for the first time proposed an equation which clarifies that the electrode impedance in the low-concentration zone (R_{LE}) is the core factor causing power density decline in large-area testing, providing crucial

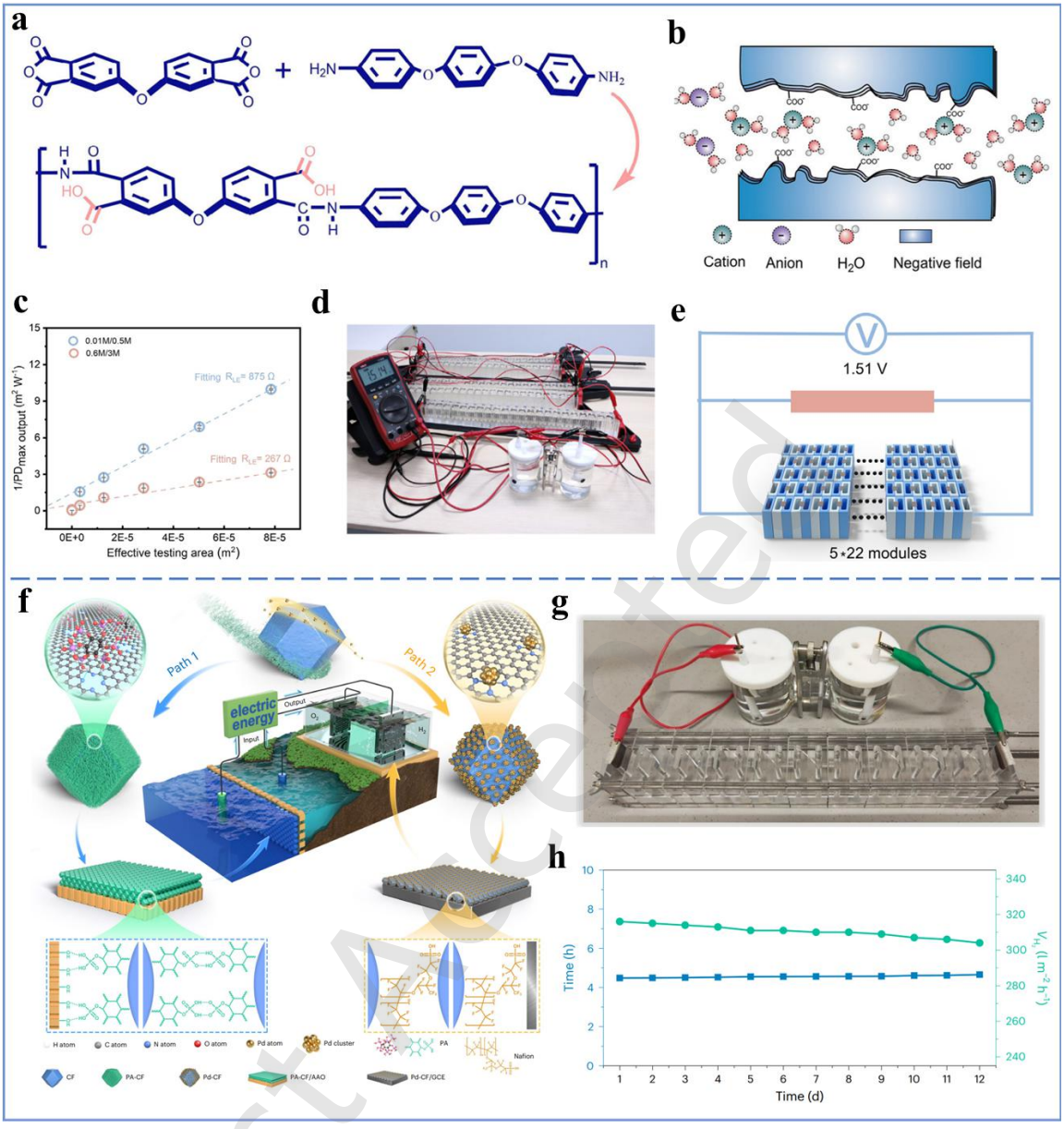

Figure 10. (a) Schematic diagram of the synthesis reaction of PAA37 membrane. (b) Schematic illustration of the ion selectivity mechanism of PAA37 membrane with high-density carboxylic acid groups and sub-nanometer channels. (c) The relationship between the maximum output power density and the effective test area. (d) Digital photograph of the series-parallel configured system (5 parallel branches, each with 22 OEPM units in series) connected with a water electrolysis device. (e) Schematic diagram of the series-parallel configuration of 110 OEPM units powering the electrolyzer to achieve 1.51 V output voltage. (Reproduced with permission from Ref [164], Copyright 2025, Wiley-VCH Verlag.) (f) Schematic diagram of the dual-path superassembly strategy for fabricating PA-CF/AAO hybrid membrane and Pd-CF/GCE hybrid electrode. (g) Digital photograph of the integrated osmotic energy-driven hydrogen production device with 10 serially connected PA-CF/AAO membrane units. (h) Long-term stability curve of hydrogen evolution rate for the integrated device with 10 serially connected PA-CF/AAO membrane units. (Reproduced with permission from Ref. [165],Copyright 2024 Springer Nature.)

theoretical basis for the design optimization of large-scale osmotic energy devices (Figure 10c). In terms of hydrogen production performance, He et al. stacked 110 PAA37-based OEPMs in series to achieve a high open-circuit voltage of 24.34 V, and adopted a hybrid series-parallel configuration (5 parallel branches with 22 OEPMs in series each) to optimize the output voltage across the electrolyzer to 1.51 V (Figure 10d and Figure 10e), which meets the voltage threshold for continuous hydrogen evolution. The PAA37 membrane achieves a power density of 6.0 $W \cdot m^{-2}$ over a

macroscopic area of 3.14 mm^2 under a 50-fold KCl concentration gradient, successfully realizing the efficient conversion from osmotic energy to hydrogen energy. However, the PAA37 membrane shows limited adaptability to pH variations and a relatively short continuous operation lifespan of 5 days, with cracks forming on the membrane surface after long-term immersion in saline solutions, which restricts its practical application in complex marine environments.

Different from the work of He et al., Liang et al.'s study [165] successfully addressed the aforementioned shortcomings, demonstrating superior adaptability to diverse pH environments and sustaining stable hydrogen production rates-two key performance metrics that He et al.'s system failed to achieve. While He et al.'s PAA37 membrane struggled with durability and narrow pH adaptability, Liang et al. overcame these limitations through innovative structural engineering and material integration, offering a more robust solution for practical osmotic energy-driven hydrogen production. They designed an osmotic energy-powered hydrogen production device by constructing core components through a dual-path superassembly strategy and completing the integration (Figure 10f): In Path 1, zeolitic imidazolate framework-8 (ZIF-8)-derived carbon framework (CF) was used as the substrate. Phytic acid (PA) combined with N atoms on the CF surface via evaporation-induced assembly to form PA-CF, which was then loaded onto an AAO substrate through fluid-oriented assembly, yielding the PA-CF/AAO ion-exchange hybrid membrane (the core of the osmotic energy generation terminal). In Path 2, Pd atoms were selectively assembled on the CF surface by adjusting pH to form Pd-CF, which was mixed with Nafion solution and deposited on a glassy carbon electrode (GCE) to obtain the Pd-CF/GCE electrocatalytic hybrid electrode, the core of the hydrogen production terminal. Finally, the two components were connected to the same circuit, enabling seamless coupling of osmotic energy generation and electrocatalytic hydrogen production without the need for external energy storage devices. Notably, the PA-CF/AAO hybrid membrane adopts an asymmetric structure, with the PA-CF layer and AAO substrate forming a Janus heterocharge distribution. The strong electronegativity and superhydrophilicity of the PA-CF layer synergize with the composite structure consisting of two-dimensional narrow channels between facets and three-dimensional sponge-like channels between vertices and facets, collectively endowing the membrane with excellent high cation selectivity. This structural design not only guides the directional and rapid transport of Na^+ but also effectively suppresses interfacial polarization, resulting in a cation transference number significantly higher than that of traditional symmetric membranes. The transport current of K^+ is consistently much higher than that of Cl^-, and the cation transport efficiency is further enhanced when the PA-CF side is at high concentration. The membrane also exhibits outstanding pH adaptability, with no significant attenuation in osmotic energy conversion power density over a wide pH range of 4~10, meaning it can stably harvest osmotic energy in seawater environments with varying acidities and alkalinities. Benefiting from these advantages, the hydrogen production terminal powered by 10 serially connected membrane units achieves a Faraday efficiency close to 100% (Figure 10g). Under artificial salinity gradient, the hydrogen evolution rate continuously exceeds 300 $L \cdot m^{-2} \cdot h^{-1}$ and remains stable for more than 12 days (Figure 10h). The output voltage of the 10 serially connected membrane units shows a good linear relationship with the number of units, stably providing a working voltage of 1.55 V for hydrogen production. Compared with traditional Pt-C/Pd-C electrocatalytic hydrogen production devices, it can save 38.08~44.02 kWh of electricity per 1 kg of hydrogen produced, demonstrating excellent practical application potential.

In summary, renewable energy-driven hydrogen production has achieved considerable progress in recent years, yet osmotic energy-powered hydrogen production remains in an emerging developmental stage with multiple challenges hindering its industrialization. Current systems mostly adopt a disconnected design where osmotic energy-harvesting devices are separated from hydrogen production units, failing to realize highly integrated device construction. Besides, the large-area and scalable preparation of high-performance ion-selective membranes still faces technical hurdles, and issues such as limited membrane stability and narrow environmental adaptability further restrict practical application. These bottlenecks in

structural design, material preparation and performance stability mean that osmotic energy-powered hydrogen production requires more in-depth research and exploration for large-scale industrial application and commercialization.

4. Conclusion and perspectives

This review systematically summarizes the fundamentals, material advances, and application progress of osmotic energy-driven self-powered sensing systems, offering strategic guidance for the development of nanofluidic-based self-sustaining technologies. First, the core energy conversion mechanisms governed by the EDL effect and ion-selective transport are outlined, clarifying the critical role of the λ_D in modulating EDL overlap and ion selectivity, alongside key thermodynamic equations describing theoretical energy conversion limits. Second, advanced nanofluidic membrane materials are categorized into 2D layered membranes and 3D porous framework membranes, with representative materials including GO membranes, MXene membranes, LDH-based membranes, HOF membranes, and MOF membranes, and their structural characteristics, ion transport properties, advantages, and inherent limitations analyzed comprehensively. Third, the core selection criteria for ion-selective membranes, including surface charge characteristics, nanochannel structural parameters, and hydrophilicity, are discussed, highlighting their synergistic regulation of ion transport efficiency and sensing performance. Following this, four typical intergrated self-powered sensing applications driven by osmotic energy are presented, including nutrient sensing, pressure sensing, humidity sensing, and image sensing, with in-depth analysis of the sensing mechanism. The transition of concentration gradient design from external environment-dependent modes to built-in gradient configurations is underscored, as this transition enhances system adaptability and stability. Additionally, other osmotic energy-driven self-powered technologies such as self-powered lithium extraction and hydrogen production are introduced as extended applications. Despite the notable advantages of osmotic energy-driven self-powered systems, challenges remain in scalable membrane fabrication, long-term operational stability, precise mechanism elucidation, and practical device integration. Addressing these challenges will be crucial for advancing the field and realizing the large-scale deployment of osmotic energy self-powered technologies in flexible electronics and sustainable energy systems.

(1) Elucidation of microscopic mechanism elucidation

Deepening the understanding of microscopic mechanisms underlying osmotic energy conversion and sensing responses is a fundamental prerequisite for optimizing system performance. Current research has preliminarily clarified the core role of the EDL effect and ion-selective transport, but many dynamic processes and interfacial interactions remain insufficiently explored. Future studies should leverage advanced in-situ characterization techniques such as synchrotron X-ray scattering, time-resolved electrochemical measurements, and Atomic Force Microscopy to track ion migration trajectories at the membrane-solution interface in real time. By monitoring the dynamic evolution of nanochannel radius and charge distribution under external stimuli including pressure, humidity and ion concentration changes the regulation law of nanochannel structure on ion transport can be accurately revealed. Additionally, combining multi-scale simulation methods from molecular dynamics to continuum mechanics can help analyze the interaction energy between membrane surface functional groups and ions as well as the steric hindrance effect during ion migration. Exploring the correlation between nanochannel size surface charge density and ion selectivity will clarify the intrinsic mechanism of energy conversion efficiency improvement. This in-depth investigation of microscopic mechanisms will provide a precise theoretical basis for the rational design of high-performance membranes and the optimization of sensing response characteristics enabling breakthroughs in the performance limitations of current systems.

(2) Exploration of suitable concentration gradient interfaces

Exploring stable accessible and environment-adaptive osmotic concentration gradient interfaces is a key challenge restricting the practical application of osmotic energy-driven self-powered systems. The core demand for gradient interfaces lies in maintaining long-term stability while adapting to diverse application scenarios. For wearable and

biomedical sensing systems research should focus on developing biocompatible gradient solutions that avoid skin irritation and microbial contamination. Designing microfluidic reservoir structures with gradient retention capabilities such as porous hydrogel-based reservoirs can reduce ion diffusion loss and extend gradient lifespan. For environmental and marine sensing, the focus should be on constructing gradient interfaces resistant to temperature fluctuations and salt concentration interference. Investigating the dynamic balance between gradient maintenance and ion consumption under different flow rates and pressure conditions can provide theoretical support for gradient interface design. Additionally developing self-regenerating gradient systems that utilize environmental substances to supplement ion loss such as extracting ions from seawater or soil can further enhance the long-term operational reliability of gradient interfaces. The successful exploration of such gradient interfaces will lay a solid foundation for the stable operation of self-powered systems in complex practical environments.

(3) Optimization of membrane material performance

Continuous optimization of nanofluidic membrane performance is the core driving force for the advancement of osmotic energy-driven self-powered technology. For two-dimensional layered membranes such as graphene oxide and MXene membranes the primary focus is to improve mechanical stability and anti-swelling properties. Cross-linking modification using organic molecules with multi-functional groups can enhance the interaction force between nanosheets reducing structural deformation under high humidity conditions. Composite strategies combining two-dimensional materials with inorganic nanoparticles or polymer matrices can simultaneously improve mechanical strength and ion selectivity. For three-dimensional porous framework membranes including hydrogen-bonded organic framework and metal-organic framework membranes the key directions are enhancing aqueous stability and reducing synthesis costs. Modifying framework ligands with hydrophobic functional groups can suppress water molecule intrusion and prevent structural collapse. Developing low-cost and scalable synthesis methods such as template-assisted batch synthesis can promote the industrial application of framework membranes. Additionally exploring novel membrane materials with intrinsic dual ion selectivity or multi-response capabilities such as light-responsive or pH-responsive membranes can expand the application boundaries of self-powered systems. The development of high-performance membranes with integrated advantages of high selectivity high permeability and long-term stability will significantly improve the comprehensive performance of osmotic energy-driven self-powered systems.

(4) Expansion of multi-scenario sensing application scope

Expanding the application scope of osmotic energy-driven self-powered sensing in diverse scenarios is crucial for realizing its practical value. For wearable healthcare sensing, research should focus on developing flexible and conformal sensing devices integrated with multiple sensing functions. Integrating nutrient sensing pressure sensing and humidity sensing into a single wearable patch can enable real-time monitoring of physiological indicators such as sweat composition skin pressure and respiratory humidity. Optimizing device thickness and flexibility to ensure comfortable wear and movement adaptability is essential. For agricultural and environmental monitoring, the focus should be on developing in-situ sensing systems with high stability and anti-interference capabilities. Integrating wireless transmission modules and low-power consumption chips can realize remote data collection and analysis. For underwater exploration and marine resource detection, developing high-pressure resistant and corrosion-resistant sensing systems is necessary. Utilizing the waterproofness of nanofluidic membranes and optimizing electrode materials to resist seawater corrosion can extend the service life of underwater sensors. Expanding the application scope of self-powered sensing in these specialized scenarios will fully leverage the technical advantages of osmotic energy-driven systems and promote their large-scale practical deployment.

(5) Integration of artificial intelligence (AI) technology

The deep integration of AI and data science can provide an efficient strategy for the development of osmotic energy self-powered systems. Using machine learning algorithms such as transfer learning and deep learning, high-precision

prediction models can be established under small-sample conditions to rapidly predict diffusion potential, output power, and energy conversion efficiency under coupled concentration and temperature fields, with computational efficiency improved by more than one million times compared with traditional numerical simulations [166]. Through descriptor importance analysis, the contribution weights of key parameters including channel size, surface charge, and concentration gradient, to output performance can be quantified, providing clear guidance for targeted optimization of nanofluidic channel structures and membrane material compositions [167]. Combined with multi-objective optimization algorithms, synergistic improvement of high-power density, high conversion efficiency, and long-term stability can be achieved, overcoming the inherent trade-off between ion selectivity and permeability. In addition, data-driven models can uncover hidden structure–performance relationships in experimental data, guiding high-throughput screening and rational design of hydrogel membranes and 2D layered membranes with high selectivity and stability [168]. In the future, combining autonomous laboratories and digital twin technologies, AI will cover the entire chain of material preparation, device assembly, system testing, and performance regulation, significantly shortening the research cycle, reducing experimental costs, and promoting the rapid development of intelligent, high-throughput, and large-scale osmotic energy self-powered sensing systems [169].

(6) Promotion of industrialization and commercialization

The practical deployment of osmotic energy-driven self- powered sensors counts on systematic pathways that bridge laboratory achievements with industrial manufacturing and market application. Scalable and cost-effective fabrication of high-performance nanofluidic membranes represents the primary prerequisite for industrialization, which demands the development of roll-to-roll deposition, continuous assembly, and large-area printing techniques to ensure batch uniformity and reduce overall production cost. In addition, standardized protocols for device integration, packaging, and interfacial connection are also required to construct modular, miniaturized, and mechanically robust systems compatible with automated industrial assembly lines. Long-term operational stability under realistic environments can be effectively improved by enhancing the structural robustness, anti-swelling capability, antifouling performance, and corrosion resistance of membrane materials, thereby extending service life in marine, soil, high-humidity, and other harsh conditions. The establishment of unified industrial standards for performance characterization, including power density, sensitivity, cycling stability, and service life, will further facilitate product certification and market access. Targeted demonstration projects in agricultural monitoring, marine environmental detection, and wearable healthcare can accelerate market validation, and gradual expansion into the Industrial Internet and intelligent infrastructure will ultimately drive the large-scale commercialization of this emerging self- powered sensing technology.

Data availability

The data that has been used is confidential.

Acknowledgements

This work was financially supported by the Natural Science Foundation of China (22479079), Natural Science Foundation of Jiangsu Province (BK20201381), Science Foundation of Nanjing University of Posts and Telecommunications (NY219144, NY221046), and the National College Student Innovation and Entrepreneurship Training Program (202310293010Z).

Declaration of Competing Interest

The authors declare that they have no known competing financial interests or personal relationships that could have appeared to influence the work reported in this paper.

Author contribution statement

Wenhao Shi: Designed the review framework, compiled data, conducted literature search and analysis, and wrote the manuscript; **Jincheng Wu**: Conducted a domain specific literature review and assisting with data collation and validation; **Zijun Li**: Conducted a domain specific literature review and assisting with data collation and validation; **Xiaoguang Hu** and **Longlu Wang**: offered in-depth analysis and contributed to the manuscript, particularly providing critical comments in the discussion section, ensuring

smooth research progress. All authors reviewed and approved the final manuscript.

Informed consent

Not applicable.

Ethics statement

Not applicable.

Use of AI statement

During the preparation of this work, the author(s) used Kimi to assist with language refinement. After using this tool, the author(s) reviewed and edited the content as needed and take(s) full responsibility for the content of the publication.

References

[1] Guo, X.;Liu, W.;Feng, Q.;Yuan, Z.;Chen, L.;Xiao, K.; Teng, C. Nanofluidic ion transport and osmotic energy conversion based on all-natural kelp membranes. *Chemical Engineering Journal* **2025**, *512*, 162363.

[2] Mao, K.;Liu, C.;Ni, A.;Wang, J.;Sun, J.;Wang, G.;Xiong, P.; Zhu, J. Optimization of ion transport in twodimensional nanofluidic membranes for osmotic energy conversion. *Materials Today* **2025**, *82*, 274-288.

[3] Wang, P.;Tao, W.;Zhou, T.;Wang, J.;Zhao, C.;Zhou, G.; Yamauchi, Y. Nanoarchitectonics in Advanced Membranes for Enhanced Osmotic Energy Harvesting. *Advanced Materials* **2024**, *36*, 202404418.

[4] Zhang, X.;Qu, Z.;Wang, Q.; Iqbal, M. Geometry design and mechanism analysis of artificial nanoroughness for enhanced osmotic energy conversion. *Energy Conversion and Management* **2022**, *273*, 116373.

[5] Chen, C.;Li, H.;Yu, Y.;Wang, Z.;Ao, M.;Yang, C.;Yao, J.; Han, L. Ammonia recovery from real biogas slurry in the up-scaled Donnan Dialysis-Osmotic Distillation membrane-based system: Performance and potentials. *Separation and Purification Technology* **2025**, *358*, 130202.

[6] Hao, W.;Yu, Y.;Gong, Y.;Wang, G. e.;Ao, M.;Han, M.;Zhang, H.;Guo, Q.;Yao, J.;Yang, Y.;Zhou, Z.; Han, L. Sustainable alternative to biological nitrogen removal: Is ammonia recovery from municipal wastewater a fantasy? *Water Research* **2026**, *290*, 125109.

[7] Lee, B.;Wang, L.;Wang, Z.;Cooper, N. J.; Elimelech, M. Directing the research agenda on water and energy technologies with process and economic analysis. *Energy & Environmental Science* **2023**, *16*, 714-722.

[8] Ma, S.;Hao, J.;Hou, Y.;Zhao, J.;Lin, C.; Sui, X. Confined amphipathic ionic-liquid regulated anodic aluminum oxide membranes with adjustable ion selectivity for improved osmotic energy conversion. *Journal of Colloid and Interface Science* **2024**, *653*, 1217-1224.

[9] Zhou, Y.; Jiang, L. Bioinspired Nanoporous Membrane for Salinity Gradient Energy Harvesting. *Joule* **2020**, *4*, 2244-2248.

[10] Kirkegaard, J. K.;Rudolph, D. P.;Nyborg, S.;Solman, H.;Gill, E.;Cronin, T.; Hallisey, M. Tackling grand challenges in wind energy through a socio-technical perspective. *Nature Energy* **2023**, *8*, 655-664.

[11] Laing, T. Solar power challenges. *Nature Sustainability* **2022**, *5*, 285-286.

[12] van Vliet, M. T. H.;Wiberg, D.;Leduc, S.; Riahi, K. Power-generation system vulnerability and adaptation to changes in climate and water resources. *Nature Climate Change* **2016**, *6*, 375-380.

[13] Veers, P.;Dykes, K.;Lantz, E.;Barth, S.;Bottasso, C. L.;Carlson, O.;Clifton, A.;Green, J.;Green, P.;Holttinen, H.;Laird, D.;Lehtomaki, V.;Lundquist, J. K.;Manwell, J.;Marquis, M.;Meneveau, C.;Moriarty, P.;Munduate, X.;Muskulus, M.;Naughton, J.;Pao, L.;Paquette, J.;Peinke, J.;Robertson, A.;Sanz Rodrigo, J.;Sempreviva, A. M.;Smith, J. C.;Tuohy, A.; Wiser, R. Grand challenges in the science of wind energy. *Science* **2019**, *366*, eaau2027.

[14] Li, S.;Wang, J.;Lv, Y.;Cui, Z.; Wang, L. Nanomaterials-Based Nanochannel Membrane for Osmotic Energy Harvesting. *Advanced Functional Materials* **2024**, *34*, 202308176.

[15] Pakulski, D.;Czepa, W.;Del Buffa, S.;Ciesielski, A.; Samori, P. Atom-Thick Membranes for Water Purification and Blue Energy Harvesting. *Advanced Functional Materials* **2020**, *30*, 1902394.

[16] Wang, P.;Tang, X.; Ren, Q. Nuclear power plant multi-grade waste heat-enhanced salinity-gradient osmotic energy conversion under reverse temperature gradients. *Energy* **2026**, *342*, 139763.

[17] Xiao, K.;Jiang, L.; Antonietti, M. Ion Transport in Nanofluidic Devices for Energy Harvesting. *Joule* **2019**, *3*, 2364-2380.

[18] Zhu, Y.;Zhan, K.; Hou, X. Interface Design of Nanochannels for Energy Utilization. *Acs Nano* **2018**, *12*, 908-911.

[19] Chen, Y.;Vepa, R.; Shaheed, M. H. Enhanced and speedy energy extraction from a scaled-up pressure retarded osmosis process with a whale optimization based maximum power point tracking. *Energy* **2018**, *153*, 618-627.

[20] Straub, A. P.;Lin, S.; Elimelech, M. Module-Scale Analysis of Pressure Retarded Osmosis: Performance Limitations and Implications for Full-Scale Operation. *Environmental Science & Technology* **2014**, *48*, 12435-12444.

[21] Yip, N. Y.;Brogioli, D.;Hamelers, H. V. M.; Nijmeijer, K. Salinity Gradients for Sustainable Energy: Primer, Progress, and Prospects. *Environmental Science & Technology* **2016**, *50*, 12072-12094.

[22] Chae, S.;Kim, H.;Hong, J. G.;Jang, J.;Higa, M.;Pishnamazi, M.;Choi, J.-Y.;Walgama, R. C.;Bae, C.;Kim, I. S.; Park, J.-S. Clean power generation from salinity gradient using reverse electrodialysis technologies: Recent advances, bottlenecks, and future direction. *Chemical Engineering Journal* **2023**, *452*, 139482.

[23] Guo, Y.;Sun, X.;Zhang, Q.;Low, Z.-X.;Wang, H.;Zhu, Y.; Jiang, L. Fabrication of heterogeneous sulfonated poly(ether ether ketone) membranes for enhanced osmotic energy harvesting. *Journal of Membrane Science* **2025**, *735*, 124518.

[24] Ren, Z.;Zhang, Q.;Yin, J.;Jia, P.;Lu, W.;Yao, Q.;Deng, M.;Gao, Y.; Liu, N. Enhancing Osmotic Energy Harvesting Through Supramolecular Design of Oxygen-Functionalized MXene with Biomimetic Ion Channels. *Advanced Functional Materials* **2024**, *34*, 202404410.

[25] Ding, L.;Xiao, D.;Lu, Z.;Deng, J.;Wei, Y.;Caro, J.; Wang, H. Oppositely Charged Ti₃C₂T_x MXene Membranes with 2D Nanofluidic Channels for Osmotic Energy Harvesting. *Angewandte Chemie-International Edition* **2020**, *59*, 8720-8726.

[26] Zhang, M.;Sheng, N.;Song, Q.;Zhang, H.;Chen, S.;Wang, H.; Zhang, K. Enhanced selective ion transport by assembling nanofibers to membrane pairs with channel-like nanopores for osmotic energy harvesting. *Nano Energy* **2022**, *103*, 107786.

[27] Rastgar, M.;Moradi, K.;Burroughs, C.;Hemmati, A.;Hoek, E.; Sadrzadeh, M. Harvesting Blue Energy Based on Salinity and Temperature Gradient: Challenges, Solutions, and Opportunities. *Chemical Reviews* **2023**, *123*, 3c00168.

[28] Yang, T.;Pang, B.;Zhang, M.;Sheng, N.;Zhang, H.; Zhang, K. Advanced ion-selective wood membranes: Leveraging aligned cellulose nanofibers for enhanced osmotic energy conversion. *Chemical Engineering Journal* **2024**, *496*, 153891.

[29] Zhou, B.;Lin, Z.;Xie, Z.;Fu, X.;Yuan, Z.;Jiao, C.;Qin, X.; Ye, D. Scalable fabrication of regenerated cellulose nanohybrid membranes integrating opposite charges and aligned nanochannels for continuous osmotic energy harvesting. *Nano Energy* **2023**, *115*, 108693.

[30] Liu, Y.;Song, J.;Liu, Z.;Chen, J.;Wang, D.;Zhi, H.;Tang, J.;Zhang, Y.;Li, N.;Zhou, W.;An, M.;Liu, H.; Xue, G. Anti-Swelling Polyelectrolyte Hydrogel with Submillimeter Lateral Confinement for Osmotic Energy Conversion. *Nano-Micro Letters* **2024**, *17*, 81.

[31] Yip, N. Y.; Elimelech, M. Comparison of Energy Efficiency and Power Density in Pressure Retarded Osmosis and Reverse Electrodialysis. *Environmental Science & Technology* **2014**, *48*, 11002-11012.

[32] Zhang, R.;Lin, Z.;Lyu, G.;Zhao, R.;Wang, X.;Wang, Z.; Yoo, C. G. Synergistic integration of redox-active nanoparticles and hierarchical porosity for high-performance osmotic energy harvesting in cellulose-based membranes. *Chemical Engineering Journal* **2025**, *520*, 165851.

[33] Emmerich, T.;Vasu, K. S.;Nigues, A.;Keerthi, A.;Radha, B.;Siria, A.; Bocquet, L. Enhanced nanofluidic transport in activated carbon nanoconduits. *Nature Materials* **2022**, *21*, 696–702.

[34] Feng, Y.;Li, S.;Lu, H.;Lei, L.;Rong, Q.;Su, Z.;Zhang, D.;Wang, X.;Wang, L.; Wang, J. Nanoarchitecture via Synchronic Stacking of Metallic and Nonmetallic Two-Dimensional Nanosheets for Optimal Light-Driven Ion Transport. *Acs Nano* **2024**, *18*, 32793-32805.

[35] Li, C.;Chen, C.;Shi, J.;Han, W.;Fu, Q.; Yang, L. Biomimetic action-potential transmission via mechano-gated potassium channels assembled by quadruple hydrogen-bonded crown ethers. *Science Advances* **2026**, *12*, eaea6329.

[36] Li, Q.;Zhou, K.;Zhu, B.;Liu, X.;Lao, J.;Gao, J.; Jiang, L. Artificial Sodium Channels for Enhanced Osmotic Energy Harvesting. *Journal of the American Chemical Society* **2023**, *145*, 28038-28048.

[37] Ling, H.;Xin, W.;Qian, Y.;He, X.;Yang, L.;Chen, W.;Wu, Y.;Du, H.;Liu, Y.;Kong, X.-Y.;Jiang, L.; Wen, L. Heterogeneous Electrospinning Nanofiber Membranes with pH-regulated Ion Gating for Tunable Osmotic Power Harvesting. *Angewandte Chemie-International Edition* **2023**, *62*, 202212120.

[38] Liu, S.-H.;Zhang, D.;Fang, Y.-P.;Liang, Z.-X.;Zhao, Z.-K.;Chen, X.-C.;Yao, J.; Jiang, L. Topologically Programmed Graphene Oxide Membranes with Bioinspired Superstructures toward Boosting Osmotic Energy Harvesting. *Advanced Functional Materials* **2023**, *33*, 202211532.

[39] Qian, H.;Fan, H.;Peng, P.;Du, Y.;Li, X.;Liu, Y.;Yang, F.;Zhou, Y.;Wang, Z. L.; Wei, D. Biomimetic Janus MXene membrane with bidirectional ion permselectivity for enhanced osmotic effects and iontronic logic control. *Science Advances* **2025**, *11*, eadx1184.

[40] Wang, J.;Wang, D.;Song, Z.;Jiang, N.;Li, S.;Zhang, Y.;Huang, B.;Zhou, H.;Cui, Z.; Wang, L. Efficient solar energy conversion via bionic sunlight-driven ion transport boosted by synergistic photo-electric/thermal effects. *Energy & Environmental Science* **2023**, *16*, 3146-3157.

[41] Zhang, J.;Zhao, N.;Jiang, X.;Li, Z.;Chen, K.;Wang, X.;Jing, T.;Guo, Y.;Xie, L.;Wu, Z.; Zhang, Z. Confined Assembly of Superwettable Nanomaterials for Bioinspired Nanofluidic Membranes/Applications. *Acs Nano* **2025**, *19*, 35193-35211.

[42] Lai, Z.;Su, H.;Xian, W.;Guo, Q.;Meng, Q.-W.;Wu, D.;Wang, S.; Sun, Q. Covalent Organic Framework Membranes with Spatially Aligned Ionic Sites Achieve Record Thermo-Osmotic Output Power Density. *Advanced Energy Materials* **2025**, *15*, 2405045.

[43] Lin, X.;Liu, P.;Xin, W.;Teng, Y.;Chen, J.;Wu, Y.;Zhao, Y.;Kong, X.-Y.;Jiang, L.; Wen, L. Heterogeneous MXene/PS-b-P2VP Nanofluidic Membranes with Controllable Ion Transport for Osmotic Energy Conversion. *Advanced Functional Materials* **2021**, *31*, 2105013.

[44] Ling, H.;Wang, Q.;Yan, Z.;Li, X.;Zou, K.;He, Y.;Li, K.;Cui, Y.;Liu, T.;Chen, W.;Du, H.;Liu, Y.;Xin, W.;Kong, X.-Y.;Jiang, L.; Wen, L. High-Efficiency Ion Transport in Ultrathin 3D Covalent Organic Framework Nanofluidics. *Angewandte Chemie-International Edition* **2025**, *64*, e202423073.

[45] Man, Z.;Safaei, J.;Zhang, Z.;Wang, Y.;Zhou, D.;Li, P.;Zhang, X.;Jiang, L.; Wang, G. Serosa-Mimetic Nanoarchitecture Membranes for Highly Efficient Osmotic Energy Generation. *Journal of the American Chemical Society* **2021**, *143*, 16206-16216.

[46] Song, J.;Zhang, Y.;Sheng, N.;Han, Z.;Qu, X.;Zhou, Z.;Lv, X.;Chen, S.; Wang, H. One-step microbial cultivated bacterial cellulose membrane with 1D/2D nanochannels for efficient osmotic energy conversion. *International Journal of Biological Macromolecules* **2025**, *306*, 141655.

[47] Tonnah, R. K.;Chai, M.;Khedri, M.;Razbin, M.;Maleki, R.;Razmjou, A.; Asadnia, M. Bilayer asymmetric-based metal-organic frameworks membrane for blue energy conversion. *Desalination* **2024**, *591*, 117968.

[48] Zhang, R.;Wang, Z.;Zhao, R.;Lin, Z.;Yoo, C. G.;Yang, G.;Chen, J.; Lyu, G. Construction of cellulose 3D network composite membrane supported by hydroxylated boron nitride with high surface charge density to achieve high-efficiency osmotic energy harvesting. *Chemical Engineering Journal* **2024**, *500*, 157000.

[49] Graf, M.;Lihter, M.;Unuchek, D.;Sarathy, A.;Leburton, J.-P.;Kis, A.; Radenovic, A. Light-Enhanced Blue Energy Generation Using MoS₂ Nanopores. *Joule* **2019**, *3*, 1549-1564.

[50] Nagakura, T.;Ishihara, K.;Furukawa, T.;Masuda, K.; Tsuda, T. Auto-regulated osmotic pump for insulin therapy by sensing glucose concentration without energy supply. *Sensors and Actuators B-Chemical* **1996**, *34*, 229-233.

[51] Pu, J.;Zhu, H.; Qu, Z. Transverse velocity regulated ionic osmotic energy conversion induced by gravitational potential energy with the mitigation of ion concentration polarization. *Chemical Engineering Journal* **2025**, *522*, 167668.

[52] Qiu, Y.;Li, P.;Zeb, M.;Guo, F.;Kim, Y.; Ma, W. Construction of Nanochannel Membranes: Asymmetric Effect and Modulation for Enhanced Osmotic Energy Conversion. *Acs Applied Materials & Interfaces* **2026**, *18*, 104-126.

[53] Su, Y.;Hou, J.;Zhao, C.;Wang, H.; Zhang, H. Engineering sub-2 nm ion-selective membranes for advancing energy generation technologies. *Materials Today* **2025**, *89*, 206-222.

[54] Wang, W.;Hao, J.;Sun, Q.;Zhao, M.;Liu, H.;Li, C.; Sui, X. Carbon nanofibers membrane bridged with graphene nanosheet and hyperbranched polymer for

high-performance osmotic energy harvesting. *Nano Research* **2023**, *16*, 1205-1211.

[55] Zhi, H.;Yan, P.;Wang, D.;Liu, Y.;Tang, J.;Yang, X.;Liu, Z.;Zhang, Y.;Li, N.;An, M.;Liu, H.; Xue, G. Large-Area Graphene-Based Ion-Selective Membranes with Micro/Meso-Pores for Osmotic Energy Harvesting. *Advanced Functional Materials* **2024**, *34*, 202401922.

[56] Dartoomi, H.;Khatibi, M.;Duval, J. F. L.; Ashrafizadeh, S. N. Surface wrinkling and roughness engineering in polyelectrolyte-coated nanofluidic channels for enhanced osmotic energy harvesting. *Desalination* **2025**, *616*, 119378.

[57] Joly, L.;Meissner, R. H.;Iannuzzi, M.; Tocci, G. Osmotic Transport at the Aqueous Graphene and hBN Interfaces: Scaling Laws from a Unified, First-Principles Description. *Acs Nano* **2021**, *15*, 15249-15258.

[58] Liu, Q.;Zhu, H.; Qu, Z. Experiment and simulation analyses of GOM based salinity gradient osmotic energy conversion with nonsymmetric photothermal effect. *Energy Conversion and Management* **2023**, *298*, 117783.

[59] Wang, T.-H.; Chang, Q.-Y. Intelligent nanochannel topology engineering via integrated machine learning and optimization for high-performance osmotic energy conversion. *Desalination* **2026**, *623*, 119801.

[60] Wu, Y.;Zhou, T.;Wang, Y.;Qian, Y.;Chen, W.;Zhu, C.;Niu, B.;Kong, X.-Y.;Zhao, Y.;Lin, X.;Jiang, L.; Wen, L. The synergistic effect of space and surface charge on nanoconfined ion transport and nanofluidic energy harvesting. *Nano Energy* **2022**, *92*, 106709.

[61] Zhang, M.;Jing, Y.;Tang, J.;Wang, S.;Liu, Z.;Liu, B.;Zheng, Z.; Zhang, Q. Unveiling Ion-Transport Dynamics in 2D Nanofluidic Anion-Selective Membranes toward Osmotic Energy Harvesting. *Nano Letters* **2025**, *25*, 13857-13865.

[62] Chu, L.;Cang, L.;Sun, Z.;Wang, X.;Fang, G.; Gao, J. Reagent-free electrokinetic remediation coupled with anode oxidation for the treatment of phenanthrene polluted soil. *Journal of Hazardous Materials* **2022**, *433*, 128724.

[63] Nagar, A.;Islam, M. R.;Joshua, K.;Gupte, T.;Jana, S. K.;Manna, S.;Thomas, T.; Pradeep, T. Ion-Exchanging Graphenic Nanochannels for Macroscopic Osmotic Energy Harvesting. *Acs Sustainable Chemistry & Engineering* **2022**, *10*, 2c04138.

[64] Bures, M.;Gotz, D.;Charvat, J.;Svoboda, M.;Pocedic, J.;Kosek, J.;Zubov, A.; Mazur, P. Evaluation of mitigation of capacity decay in vanadium redox flow batteries for cation- and anion-exchange membrane by validated mathematical modelling. *Journal of Power Sources* **2024**, *591*, 233769.

[65] Eti, M.;Cihanoglu, A.;Hamaloglu, K. O.;Altiok, E.;Guler, E.;Tuncel, A.; Kabay, N. Synthesis of Silver Nanoparticle-Immobilized Antibacterial Anion-Exchange Membranes for Salinity Gradient Energy Production by Reverse Electrodialysis. *Acs Sustainable Chemistry & Engineering* **2024**, *12*, 3977-3986.

[66] Hao, J.;Ning, Y.;Hou, Y.;Ma, S.;Lin, C.;Zhao, J.;Li, C.; Sui, X. Polydopamine functionalized graphene oxide membrane with the sandwich structure for osmotic energy conversion. *Journal of Colloid and Interface Science* **2023**, *630*, 795-803.

[67] Yang, Z.-J.;Yeh, L.-H.;Peng, Y.-H.;Chuang, Y.-P.; Wu, K. C. W. Enhancing Ionic Selectivity and Osmotic Energy by Using an Ultrathin Zr-MOF-Based Heterogeneous Membrane with Trilayered Continuous Porous Structure. *Angewandte Chemie-International Edition* **2024**, *63*, e202408375.

[68] Qin, S.;Yang, G.;Wang, S.;Ma, Y.;Wang, Z.;Wang, L.;Liu, D.; Lei, W. Tunable Surface Charge of Layered Double Hydroxide Membranes Enabling Osmotic Energy Harvesting from Anion Transport. *Small* **2024**, *20*, 202400850.

[69] Liu, Y.;Ping, J.; Ying, Y. Anion-Selective Layered Double Hydroxide Composites-Based Osmotic Energy Conversion for Real-Time Nutrient Solution Detection. *Advanced Science* **2022**, *9*, 2103696.

[70] Baosen Zhang, Y. J., Tianci Ren, Baojin Chen, Renyun Zhang and Yanchao Mao Recent advances in nature inspired triboelectric nanogenerators for self-powered systems. *International Journal of Extreme Manufacturing* **2024**, *6*, 062003.

[71] Lin, Z.;Wang, Y.;Nie, S.;Zou, M.;Xu, F.;Deng, Y.;Lu, Y.;Deng, L.;Li, M.;Luo, G.;Dong, T.;Zhao, L.; Guo, H. Island-bridge microstructured triboelectric pressure sensor for effective dynamic epidermal pulse monitoring. *Soft Science* **2025**, *5*, 47.

[72] He, X.;Zi, Y.;Yu, H.;Zhang, S. L.;Wang, J.;Ding, W.;Zou, H.;Zhang, W.;Lu, C.; Wang, Z. L. An ultrathin paper-based self-powered system for portable electronics and wireless human-machine interaction. *Nano Energy* **2017**, *39*, 328-336.

[73] Wei, S.;Li, Z.;Murugappan, K.;Li, Z.;Zhang, F.;Saraswathyvilasam, A. G.;Lysevych, M.;Tan, H. H.;Jagadish, C.;Tricoli, A.; Fu, L. A Self-Powered Portable Nanowire Array Gas Sensor for Dynamic NO₂ Monitoring at Room Temperature. *Advanced Materials* **2023**, *35*, 202207199.

[74] Ferreira, G.;Opiniao, A.;Das, S.;Goswami, S.;Pereira, L.;Nandy, S.;Martins, R.; Fortunato, E. Smart IoT enabled interactive self-powered security tag designed with functionalized paper. *Nano Energy* **2022**, *95*, 107021.

[75] Liu, C.;Gu, R.;Yang, J.;Luo, L.;Chen, M.;Xiong, Y.;Huo, Z.;Liu, Y.;Zhang, K.;Gong, J.;Wei, L.;Lei, Y.;Wang, Z. L.; Sun, Q. A Self-Powered Dual Ratchet Angle Sensing System for Digital Twins and Smart Healthcare. *Advanced Functional Materials* **2024**, *34*, 202405104.

[76] Ma, H.;Liu, Q.;Cheng, P.;Shen, L.;Ma, J.;Lv, F.;Zhang, Y.;Jiang, Y.;Sun, T.; Zhu, N. Wearable Motion Smartsensors Self-Powered by Core-Shell Au@Pt Methanol Fuel Cells. *Acs Sensors* **2021**, *6*, 4526-4534.

[77] Tang, W.;Sun, Q.; Wang, Z. L. Self-Powered Sensing in Wearable Electronics-A Paradigm Shift Technology. *Chemical Reviews* **2023**, *123*, 12105-12134.

[78] Lu, L.;Wu, J.;Zhang, Y.;Liu, C.;Hu, Y.;Chen, B.;Zhu, Y.; Mao, Y. Noncontact 3D gesture recognition enabled VR human-machine interface via electret-nanofiber-based triboelectric sensor. *Nano Research* **2025**, *18*, 94907924.

[79] Xinxin He, Z. L., Xingcan Huang, Qiang Zhang, Yuyang Zeng, Jialin Li, Chun Ki Yiu, Yawen Yang, Jingkun Zhou, Guoqiang Xu, Jiachen Wang, Jian Li, Zitong Xu, Zhenlin Chen, Yiming Liu, Yuyu Gao, Binbin Zhang, Guangyao Zhao, Zhan Gao, Pengcheng Wu, Rui Shi, Yuze Qiu, Hehua Zhang, Lung Chow, Denglin Ye, Ya Huang and Xinge Yu Sweat-powered, skin-adhesive multimodal sensor for longterm and real-time sweat monitoring. *BMEMat* **2025**, *3*, http://doi.org/1002/bmm1002.12124.

[80] Pan, J.;Xu, W.;Zhang, Y.;Ke, Y.;Dong, J.;Li, W.;Wang, L.;Wang, B.;Meng, B.;Zhou, Q.; Xia, F. Osmotic energy-based systems for self-powered sensing. *Nano Energy* **2024**, *132*, 110412.

[81] Yu, G.;Zhang, Q.;Wang, M.;Lu, H.;Chen, Z.;Liu, J.;Chen, C.;Wang, S.;Ma, Y.; Yue, Y. Osmotic Energy Directly Driving Flexible All-Solid-State 2D Nanofluidic Pressure Sensors. *Advanced Materials* **2025**, *37*, e06990.

[82] Zu, L.;Liu, D.;Shao, J.;Liu, Y.;Shu, S.;Li, C.;Shi, X.;Chen, B.; Wang, Z. L. A Self-Powered Early Warning Glove with Integrated Elastic-Arched Triboelectric Nanogenerator and Flexible Printed Circuit for Real-Time Safety Protection. *Advanced Materials Technologies* **2022**, *7*, 2100787.

[83] Zhang, D.;Zhou, L.;Wu, Y.;Yang, C.; Zhang, H. Triboelectric Nanogenerator for Self-Powered Gas Sensing. *Small* **2024**, *20*, 2406964.

[84] Liu, Q.;Wang, Q.;Qu, Z.; Zhang, J. Interfacial binding rope theory of ion transport in sub-nanochannels and its application for osmotic energy conversion. *Nano Energy* **2023**, *113*, 108545.

[85] Wang, Q.;Qu, Z.; Jiang, J. Sub-nanometer resolution for anion conduction in a covalent-organic framework membrane: A hierarchical approach. *Journal of Energy Chemistry* **2026**, *113*, 186-197.

[86] Cui, G.;Xu, Z.;Zhang, S.;Siria, A.; Ma, M. Coupling between ion transport and electronic properties in individual carbon nanotubes. *Science Advances* **2025**, *11*, eadu7410.

[87] Guo, Y.;Zhang, X.;Zhou, S.;Liang, Q.;Zeng, H.;Xu, Y.;Awati, A.;Liang, K.;Zhu, D.;Liu, M.;Jiang, L.; Kong, B. Super-Assembled Lamellar Conductive Heterochannels with Optical-Electrical Coupling Sensitivity for Smart Ion Transport. *Angewandte Chemie-International Edition* **2025**, *64*, e202500116.

[88] Yin, J.;Jia, P.;Ren, Z.;Zhang, Q.;Lu, W.;Yao, Q.;Deng, M.;Zhou, X.;Gao, Y.; Liu, N. Mechanically Enhanced, Environmentally Stable, and Bioinspired Charge-Gradient Hydrogel Membranes for Efficient Ion Gradient Power Generation and Linear Self-Powered Sensing. *Advanced Materials* **2025**, *37*, 202417944.

[89] Wang, Q.; Qu, Z. Localized insight into potential-switched structure and hierarchical transport of water-in-salt electrolyte at electrified interfaces. *Energy Storage Materials* **2026**, *86*, 104959.

[90] Wang, Q.;Qu, Z.; Tian, D. Electric Double Layer Theory

of Interfacial Ionic Liquids for Capturing Ion Hierarchical Aggregation and Anisotropic Dynamics. *Advanced Energy Materials* **2025**, *15*, 202402974.

[91] Pang, S.;Dai, L.;Yi, Z.;Qu, K.;Wang, Y.;Wu, Y.;Fang, C.;Huang, K.; Xu, Z. 2D nanofluidic vermiculite membranes with self-confinement channels and recognition sites for ultrafast lithium ion-selective transport. *Journal of Membrane Science* **2023**, *687*, 122054.

[92] Chu, C.-W.;Fauziah, A. R.; Yeh, L.-H. Optimizing Membranes for Osmotic Power Generation. *Angewandte Chemie-International Edition* **2023**, *62*, e202303582.

[93] Liu, X.;Li, X.;Chu, X.;Zhang, B.;Zhang, J.;Hambsch, M.;Mannsfeld, S. C. B.;Borrelli, M.;Loeffler, M.;Pohl, D.;Liu, Y.;Zhang, Z.; Feng, X. Giant Blue Energy Harvesting in Two-Dimensional Polymer Membranes with Spatially Aligned Charges. *Advanced Materials* **2024**, *36*, 2310791.

[94] Hu, Y.;Xiao, H.;Fu, L.;Liu, P.;Wu, Y.;Chen, W.;Qian, Y.;Zhou, S.;Kong, X.-y.;Zhang, Z.;Jiang, L.; Wen, L. Confined Ionic-Liquid-Mediated Cation Diffusion through Layered Membranes for High-Performance Osmotic Energy Conversion. *Advanced Materials* **2023**, *35*, 202301285.

[95] Qian, H.;Peng, P.;Fan, H.;Yang, Z.;Yang, L.;Zhou, Y.;Tan, D.;Yang, F.;Willatzen, M.;Amaratunga, G.;Wang, Z.; Wei, D. Horizontal Transport in Ti₃C₂T_x MXene for Highly Efficient Osmotic Energy Conversion from Saline-Alkali Environments. *Angewandte Chemie-International Edition* **2024**, *63*, e202414984.

[96] Koudahi, M. F.; Frackowiak, E. Ti₃C₂T_x MXene as Intriguing Material for Electrochemical Capacitor. *Small* **2024**, *20*, 2307165.

[97] Huang, H.; Yang, W. MXene-Based Micro-Supercapacitors: Ink Rheology, Microelectrode Design and Integrated System. *Acs Nano* **2024**, *18*, 4651-4682.

[98] Li, F.;Jiang, X.;Zhao, J.; Zhang, S. Graphene oxide: A promising nanomaterial for energy and environmental applications. *Nano Energy* **2015**, *16*, 488-515.

[99] Shah, I. A.;Bilal, M.;Almanassra, I. W.; Ihsanullah, I. A comprehensive review of graphene oxide-based membranes for efficient dye removal from water sources. *Separation and Purification Technology* **2024**, *330*, 125277.

[100] Chen, G.;Zhai, S.;Zhai, Y.;Zhang, K.;Yue, Q.;Wang, L.;Zhao, J.;Wang, H.;Liu, J.; Jia, J. Preparation of sulfonic-functionalized graphene oxide as ion-exchange material and its application into electrochemiluminescence analysis. *Biosensors & Bioelectronics* **2011**, *26*, 3136-3141.

[101] Yuan, Y.;Gao, X.;Wei, Y.;Wang, X.;Wang, J.;Zhang, Y.; Gao, C. Enhanced desalination performance of carboxyl functionalized graphene oxide nanofiltration membranes. *Desalination* **2017**, *405*, 29-39.

[102] Hu, J.;Zhang, Y.; Dong, M. Recent Advances in Layered Double Hydroxides Membranes: Insights into Multiple Mass Transport. *Advanced Functional Materials* **2024**, *34*, 2312452.

[103] Ni, H.;Wang, N.;Yang, Y.;Shen, M.; An, Q.-F. Positively-charged nanofiltration membrane constructed by polyethyleneimine/layered double hydroxide for Mg²⁺/Li⁺ separation. *Desalination* **2023**, *548*, 116256.

[104] Lei, J.;Xiong, Y.;Yu, F.; Ma, J. Flexible self-supporting CoFe-LDH/MXene film as a chloride ions storage electrode in capacitive deionization. *Chemical Engineering Journal* **2022**, *437*, 135381.

[105] Zhang, F.;Sun, M.;Xu, S.;Zhao, L.; Zhang, B. Fabrication of oriented layered double hydroxide films by spin coating and their use in corrosion protection. *Chemical Engineering Journal* **2008**, *141*, 362-367.

[106] Du, M.;Ye, W.;Fu, H.;Lv, W.; Zheng, Q. Direct growth of layered double hydroxides in an aqueous suspension of carbon nanotubes and their application as fillers in polypropylene. *Composites Science and Technology* **2014**, *105*, 28-36.

[107] Tamadoni Saray, M.;Yurkiv, V.; Shahbazian-Yassar, R. In Situ Thermolysis of a Ni Salt on Amorphous Carbon and Graphene Oxide Substrates. *Advanced Functional Materials* **2023**, *33*, 2213747.

[108] Yun, T.;Lee, G. S.;Choi, J.;Kim, H.;Yang, G. G.;Lee, H. J.;Kim, J. G.;Lee, H. M.;Koo, C. M.;Lim, J.; Kim, S. O. Multidimensional

Ti₃C₂T_x MXene Architectures via Interfacial Electrochemical Self-Assembly. *Acs Nano* **2021**, *15*, 10058-10066.

[109] He, Y.;Xiao, T.;Lu, B.;Li, X.;Zhang, C.;He, J.;Zhai, J.; Fan, X. Hydrogen-Bonded Organic Framework Nanochannels for Salinity Gradient Energy Conversion. *Acs Applied Energy Materials* **2022**, *5*, 13773–13779.

[110] Liu, Y.-C.;Yeh, L.-H.;Zheng, M.-J.; Wu, K. C. W. Highly selective and high-performance osmotic power generators in subnanochannel membranes enabled by metal-organic frameworks. *Science Advances* **2021**, *7*, eabe9924.

[111] Chen, C.;Shen, L.;Lin, H.;Zhao, D.;Li, B.; Chen, B. Hydrogen-bonded organic frameworks for membrane separation. *Chemical Society Reviews* **2024**, *53*, 2738-2760.

[112] Muthu, D.;Dharman, R. K.;Muthu, S. E.; Oh, T. H. Recent developments in metal-organic framework-derived transition metal oxide@carbon nanostructure and carbon nanostructure for supercapacitor applications. *Journal of Energy Storage* **2025**, *119*, 116365.

[113] Elboughdiri, N.;Kriaa, K.;Maatki, C.;Fatimah, S.;Chaouiki, A.;Chafiq, M.; Ko, Y. G. Engineering hydrogen-bonded organic frameworks: Pioneering membrane materials for advanced separation. *Separation and Purification Technology* **2025**, *370*, 133205.

[114] Yang, Y.;Sun, Z.;Wu, Y.;Liang, Z.;Li, F.;Zhu, M.; Liu, J. Porous Organic Framework Materials (MOF, COF, and HOF) as the Multifunctional Separator for Rechargeable Lithium Metal Batteries. *Small* **2024**, *20*, 202401457.

[115] Wang, Y.-B.;Lin, Y.-X.;Wang, J.-X.;Zhang, X.;Wu, H.;Zhou, W.;Chen, B.;Qian, G.; Li, B. A Microporous Hydrogen-Bonded Organic Framework with Alkynyl Sites for Highly Efficient Propane/Propylene Separation. *Journal of the American Chemical Society* **2025**, *147*, 24403-24412.

[116] Yang, S.;Peng, L.;Sun, D. T.;Asgari, M.;Oveisi, E.;Trukhina, O.;Bulut, S.;Jamali, A.; Queen, W. L. A new post-synthetic polymerization strategy makes metal-organic frameworks more stable. *Chemical Science* **2019**, *10*, 4542-4549.

[117] Cheng, W.;Xu, C.;Zhang, Q.;Yue, Y.;Lei, D.;Wen, L.; Wang, S. Ion Concentration Gradient Induced Efficient Ion Migration in Hydrogen-Bonded Organic Frameworks for High-Performance, Self-Powered Humidity Sensing. *Small* **2025**, *21*, 2412497.

[118] Colotti, A.;Fontan, J. G.;Goldsztejn, A.;Briot, S.;Chaumette, F.;Kermorgant, O.; El Din, M. S. Determination of All Stable and Unstable Equilibria for Image-Point-Based Visual Servoing. *Ieee Transactions on Robotics* **2024**, *40*, 3406-3424.

[119] Jaffe, L.;Zelinski, M.; Sakla, W. Remote Sensor Design for Visual Recognition With Convolutional Neural Networks. *Ieee Transactions on Geoscience and Remote Sensing* **2019**, *57*, 9090-9108.

[120] Song, Y.-Z.;Bowen, C. R.;Kim, A. H.;Nassehi, A.;Padget, J.; Gathercole, N. Virtual visual sensors and their application in structural health monitoring. *Structural Health Monitoring-an International Journal* **2014**, *13*, 251-264.

[121] High frame rate multi-resonance imaging refractometry with distributed feedback dye laser sensor. *Light:Science & Applications* **2015**, *4*, e269.

[122] Nie, K.;Shi, X.;Cheng, S.;Gao, Z.; Xu, J. High Frame Rate Video Reconstruction and Deblurring Based on Dynamic and Active Pixel Vision Image Sensor. *Ieee Transactions on Circuits and Systems for Video Technology* **2021**, *31*, 2938-2952.

[123] Lu, F.;Shen, K.;Yuan, G.;Qiao, S.;Hu, C.; Lyu, Z. An Autonomous Vehicle Collaborative Perception Method Based on Holographic Counterpart Construction From Consumer Electronics Sensors. *Ieee Transactions on Consumer Electronics* **2025**, *71*, 8571-8581.

[124] Zhong, S.; Ali, R. Joint Self-Attention Mechanism and Residual Network for Automated Monitoring of Intelligent Sensor in Consumer Electronics. *Ieee Transactions on Consumer Electronics* **2024**, *70*, 1302-1309.

[125] Huang, Y.;Wu, C.;Cao, Y.;Zheng, J.;Zeng, B.;Li, X.;Li, M.; Tang, J. Scalable integration of photoresponsive highly aligned nanochannels for self-powered ionic devices. *Science Advances* **2024**, *10*, eads5591.

[126] Abu, S. M.;Hannan, M. A.;Lipu, M. S. H.;Ker, P. J.;Hossain, M. J.; Mahlia, T. M. I. State of the art of lithium-ion battery material potentials: An analytical evaluations, issues and future research directions. *Journal of Cleaner Production* **2023**, *394*, 136246.

[127] Chang, X.;Zhao, Y.-M.;Yuan, B.;Fan, M.;Meng, Q.;Guo, Y.-G.; Wan, L.-J. Solid-state lithium-ion batteries for grid energy storage: opportunities and challenges. *Science China-Chemistry* **2024**, *67*, 43-66.

[128] Harper, G.;Sommerville, R.;Kendrick, E.;Driscoll, L.;Slater, P.;Stolkin, R.;Walton, A.;Christensen, P.;Heidrich, O.;Lambert, S.;Abbott, A.;Ryder, K. S.;Gaines, L.; Anderson, P. Recycling lithium-ion batteries from electric vehicles. *Nature* **2019**, *575*, 75-86.

[129] Degen, F.;Winter, M.;Bendig, D.; Tuebke, J. Energy consumption of current and future production of lithium-ion and post lithium-ion battery cells. *Nature Energy* **2023**, *8*, 1284-1295.

[130] Greim, P.;Solomon, A. A.; Breyer, C. Assessment of lithium criticality in the global energy transition and addressing policy gaps in transportation. *Nature Communications* **2020**, *11*, 4570.

[131] Castelvecchi, D. ELECTRIC CARS: THE BATTERY CHALLENGE. *Nature* **2021**, *596*, 336-339.

[132] Speirs, J.;Contestabile, M.;Houari, Y.; Gross, R. The future of lithium availability for electric vehicle batteries. *Renewable & Sustainable Energy Reviews* **2014**, *35*, 183-193.

[133] An, S.;Li, Z.;Wang, X.;Xu, T.;Feng, L.; Lai, Z. Synthesis of 100 -only LiFePO₄ nanosheets for efficient electrochemical lithium extraction from low-grade brines. *Nature Water* **2025**, *3*.

[134] Liu, C.;Li, Y.;Lin, D.;Hsu, P.-C.;Liu, B.;Yan, G.;Wu, T.;Cui, Y.; Chu, S. Lithium Extraction from Seawater through Pulsed Electrochemical Intercalation. *Joule* **2020**, *4*, 1459-1469.

[135] Wang, Y.;Zheng, X.;Lv, W.;Li, L.;Cao, H.; Sun, Z. A three-in-one strategy for lithium recovery and upcycling of spent cathode materials. *Nature Communications* **2026**, *17*, 1153.

[136] Shi, Q.;Guo, Y.;Zhang, F.;Gao, F.;Li, J.;Yang, C.;Tiraferri, A.;Ma, J.; Liu, B. Recent advances in lithium extraction from brine via solar-driven interfacial evaporation: Advanced strategies and challenges. *Water Research* **2026**, *292*, 125292.

[137] Xing, W.;Wang, D.;Feng, K.;Ding, S.;Zhang, X.;Xu, H.;Gong, J.;Qu, J.; Niu, R. Interfacial solar evaporation-driven lithium extraction from salt-lake brines for battery-grade Li₂CO₃ production. *Energy & Environmental Science* **2025**, *18*, 10102-10111.

[138] Deng, G.;Jiang, R.;Tang, F.;Hou, Z.; Feng, Y. Preparation of porous hydrophilic ion sieves for lithium recovery from highly alkaline lithium precipitation mother liquor and low-lithium raw brine: Batch and continuous operation. *Desalination* **2025**, *614*, 119159.

[139] Nikkhah, H.;Ipekci, D.;Xiang, W.;Stoll, Z.;Xu, P.;Li, B.;McCutcheon, J. R.; Beykal, B. Challenges and opportunities of recovering lithium from seawater, produced water, geothermal brines, and salt lakes using conventional and emerging technologies. *Chemical Engineering Journal* **2024**, *498*, 155349.

[140] Cheng, Y.;Nie, A.;Gan, L.-Y.;Zhang, Q.; Schwingenschloegl, U. A global view of the phase transitions of SnO₂ in rechargeable batteries based on results of high throughput calculations. *Journal of Materials Chemistry A* **2015**, *3*, 19483-19489.

[141] Wang, P.;Zhou, S.;Fu, Y.;Fang, H.;Gu, S.; Yu, J. Thermodynamic corrections of high salinity system for selective lithium extraction from brines with LiMn₂O₄/ λ -MnO₂. *Desalination* **2024**, *581*.

[142] Liu, Y.;Ran, J.;Guo, Q.;Gao, L.;Yin, S.;Li, S.;Jiang, X.;Zhang, N.; Zhou, G. Advancements in nanofiltration fouling phenomenon: From water treatment to salt lakes environments. *Desalination* **2024**, *583*, 117649.

[143] Song, H.;Su, J.; Wang, C. Multi-Ions Electrolyte Enabled High Performance Voltage Tailorable Room-Temperature Ca-Metal Batteries. *Advanced Energy Materials* **2021**, *11*, 2003685.

[144] Wohrlin, P.-L.;La Mantia, F.;Koschikowski, J.;Winter, D.; Santos, C. Fully automated flow-by reactor for direct lithium recovery based on electrochemical ion pumping. *Separation and Purification Technology* **2026**, *391*, 137055.

[145] Zhang, G.;Li, Y.;Guan, X.;Hu, G.;Su, H.;Xu, X.;Feng, G.;Shuchi, S. B.;Kim, S. C.;Zhou, J.;Xu, R.;Xiao, X.;Wu, A.; Cui, Y. Spontaneous lithium extraction and enrichment from brine with net energy output driven by counter-ion gradients. *Nature Water* **2024**, *2*, 1091-1101.

[146] Li, Z.;Chen, I. C.;Cao, L.;Liu, X.;Huang, K.-W.; Lai, Z.

Lithium extraction from brine through a decoupled and membrane-free electrochemical cell design. *Science* **2024**, *385*, 1438-1444.

[147] Yang, W.;Bao, J.;Liu, H.;Zhang, J.; Guo, L. Low-grade heat to hydrogen: Current technologies, challenges and prospective. *Renewable & Sustainable Energy Reviews* **2023**, *188*, 113842.

[148] Zhu, C.;Guan, B.;Zhuang, Z.;Chen, J.;Ma, Z.;Hu, X.;Zhao, S.;Shu, K.;Dang, H.;Gao, J.;Zhu, T.; Huang, Z. Research status and advances of ammonia and hydrogen in the field of energy: Combined utilization. *Energy Conversion and Management* **2025**, *327*, 119610.

[149] Zeyen, E.;Victoria, M.; Brown, T. Endogenous learning for green hydrogen in a sector-coupled energy model for Europe. *Nature Communications* **2023**, *14*, 3743.

[150] Ma, Y.;Wang, X. R.;Li, T.;Zhang, J.;Gao, J.; Sun, Z. Y. Hydrogen and ethanol: Production, storage, and transportation. *International Journal of Hydrogen Energy* **2021**, *46*, 27330-27348.

[151] Navarro, R. M.;Pena, M. A.; Fierro, J. L. G. Hydrogen production reactions from carbon feedstocks:: Fossils fuels and biomass. *Chemical Reviews* **2007**, *107*, 3952-3991.

[152] Busch, P.;Kendall, A.; Lipman, T. A systematic review of life cycle greenhouse gas intensity values for hydrogen production pathways. *Renewable & Sustainable Energy Reviews* **2023**, *184*, 113588.

[153] Ahn, D.;Noh, W.;Park, J.; Lee, I. Cryogenic carbon capture as the bridge for integrating hydrogen production and Liquefaction: Enhancing the sustainability of blue hydrogen Production-to-Storage systems. *Chemical Engineering Journal* **2025**, *504*, 158811.

[154] Du, T.;Xu, Y.;Ma, H.;Li, Y.;Li, Z.; Wang, C. Performance assessment of photovoltaic/thermal module coupled PEM electrolyzer hydrogen production system based on nanofluids and composite phase change materials. *Applied Energy* **2026**, *402*, 126990.

[155] Tian, W.-W.;Ying, Y.-D.;Ren, J.-T.; Yuan, Z.-Y. A trifunctional Co_{0.85}Se/NC collaborated electrocatalyst enables a self-powered energy system for uninterrupted H₂ production. *Journal of Materials Chemistry A* **2023**, *11*, 8024-8037.

[156] Attia, A. M.;Darghouth, M. N.;Ghaithan, A. M.;Mohammed, A.;Abdel-Aal, M. A. M.;Al Hanbali, A.; Alsawafy, O. G. Design optimization of standalone photovoltaic systems for enhanced energy density. *Renewable Energy* **2025**, *252*, 123506.

[157] Deng, B.;Yu, G.;Zhao, W.;Long, Y.;Yang, C.;Du, P.;He, X.;Zhang, Z.;Huang, K.;Li, X.; Wu, H. A self-circulating pathway for the oxygen evolution reaction. *Energy & Environmental Science* **2023**, *16*, 5210-5219.

[158] Smith, R. D. L.; Berlinguette, C. P. Accounting for the Dynamic Oxidative Behavior of Nickel Anodes. *Journal of the American Chemical Society* **2016**, *138*, 1561-1567.

[159] Liu, S.-Q.;Xie, S.;Wu, S.;Yang, Y.;Lei, P.-X.;Luo, S.;Feng, R.;Fu, X.-Z.; Luo, J.-L. Self-Powered System for H₂ Production and Biomass Upgrading. *Advanced Functional Materials* **2024**, *34*, 202404105.

[160] Ma, F.;Wu, Y.;Dai, S.;Lin, P.;Sun, J.; Dong, L. A soft-contact hybrid electromagnetic-triboelectric nanogenerator for self-powered water splitting towards hydrogen production. *Nano Research* **2024**, *17*, 6567-6574.

[161] Ock, I. W.;Zhao, X.;Tat, T.;Xu, J.; Chen, J. Harvesting Hydropower via a Magnetoelastic Generator for Sustainable Water Splitting. *Acs Nano* **2022**, *16*, 16816-16823.

[162] Ock, I. W.;Zhou, Y.;Zhao, X.;Manshaii, F.; Chen, J. Harvesting Ocean Wave Energy via Magnetoelastic Generators for Self-Powered Hydrogen Production. *Acs Energy Letters* **2024**, *9*, 1701-1709.

[163] Tang, W.;Han, Y.;Han, C. B.;Gao, C. Z.;Cao, X.; Wang, Z. L. Self-Powered Water Splitting Using Flowing Kinetic Energy. *Advanced Materials* **2015**, *27*, 272-276.

[164] He, J.;Li, X.;Li, W.;Zhai, J.; Fan, X. Self-Powered Green Hydrogen Production via Osmotic Energy Harvesting. *Advanced Materials* **2026**, *38*, 202514316.

[165] Liang, Q.;Huang, Y.;Guo, Y.;Zhang, X.;Hu, X.;Zeng, H.;Liang, K.;Zhao, D.;Jiang, L.; Kong, B. Efficient osmosis-powered production of green hydrogen. *Nature Sustainability* **2024**, *7*, 628–639.

[166] Zhu, H.;Qu, Z.;Guo, Z.; Zhang, J. Transfer learning-based prediction and evaluation for ionic osmotic energy conversion under concentration and temperature gradients. *Applied Energy* **2025**, *386*, 125574.

[167] Mohan, B.;Singh, K.;Ahmadov, E.;Pombeiro, A. J. L.;

Ren, P. Harvesting sustainable osmotic energy: the art of nanofluidic hydrogel membranes. *Journal of Energy Chemistry* **2025**, *105*, 577-594.

[168] Zhu, H.;Qu, Z.;Guo, Z.; Zhang, J. Data-driven framework for general explicit formula of ionic thermoregulated osmotic energy conversion based on similarity principle and deep learning. *Nano Energy* **2024**, *128*, 109955.

[169] Ling, H.;Xin, W.;Kong, X.-Y.;Jiang, L.; Wen, L. Engineering Biomimetic Nanofluidics Toward High-Performance Osmotic Energy Harvesting. *Advanced Materials* **2025**, *37*, 202506029.